

A Climatology of Quasi-Linear Convective Systems and Their Hazards in the United States

WALKER S. ASHLEY

Department of Geographic and Atmospheric Sciences, Northern Illinois University, DeKalb, Illinois

ALEX M. HABERLIE

Department of Geography and Anthropology, Louisiana State University, Baton Rouge, Louisiana

JACOB STROHM

Department of Geographic and Atmospheric Sciences, Northern Illinois University, DeKalb, Illinois

(Manuscript received 25 January 2019, in final form 16 August 2019)

ABSTRACT

This research uses image classification and machine learning methods on radar reflectivity mosaics to segment, classify, and track quasi-linear convective systems (QLCSs) in the United States for a 22-yr period. An algorithm is trained and validated using radar-derived spatial and intensity information from thousands of manually labeled QLCS and non-QLCS event slices. The algorithm is then used to automate the identification and tracking of over 3000 QLCSs with high accuracy, affording the first, systematic, long-term climatology of QLCSs. Convective regions determined by the procedure to be QLCSs are used as foci for spatiotemporal filtering of observed severe thunderstorm reports; this permits an estimation of the number of severe storm hazards due to this morphology. Results reveal that nearly 32% of MCSs are classified as QLCSs. On average, 139 QLCSs occur annually, with most of these events clustered from April through August in the eastern Great Plains and central/lower Mississippi and Ohio River Valleys. QLCSs are responsible for a spatiotemporally variable proportion of severe hazard reports, with a maximum in QLCS-report attribution (30%–42%) in the western Ohio and central Mississippi River Valleys. Over 21% of tornadoes, 28% of severe winds, and 10% of severe hail reports are due to QLCSs across the central and eastern United States. The proportion of QLCS-affiliated tornado and severe wind reports maximize during the overnight and cool season, with more than 50% of tornadoes and wind reports in some locations due to QLCSs. This research illustrates the utility of automated storm-mode classification systems in generating extensive, systematic climatologies of phenomena, reducing the need for time-consuming and spatiotemporal-limiting methods where investigators manually assign morphological classifications.

1. Introduction

The quasi-linear convective system (QLCS) is a type of MCS (cf. Houze 2018) that features a convective line or line segments that are much longer than they are wide. The QLCS (Weisman and Davis 1998) includes many system types that have been labeled as squall-line MCSs (Newton 1950), leading-line/trailing-stratiform MCSs (Houze et al. 1990; Parker and Johnson 2000), line echo wave patterns (LEWPs; Nolen 1959), persistent elongated convective systems (PECSs; Anderson and Arritt 1998; Jirak et al. 2003), and bow echoes (Fujita

1978; Przybylinski 1995; Weisman 2001). These linear-oriented convective morphologies occur across a broad spectrum of environmental conditions, sometimes developing quickly in environments with strong, external forcing (Newton 1950; Heymsfield and Schotz 1985; Dial et al. 2010), and, in other cases, more slowly through the upscale growth of individual cells and subsequent internal, cold pool dynamics (Weisman 1992; Weisman and Rotunno 2004) and/or gravity waves (Carbone et al. 1990; Crook et al. 1990; Carbone et al. 2002). Though the QLCS has not received as much attention as the supercell in the literature, there has been considerable growth in observational, field campaign (e.g., Davis et al. 2004; Geerts et al. 2017), climatological, numerical modeling,

Corresponding author: Walker S. Ashley, washley@niu.edu

DOI: 10.1175/WAF-D-19-0014.1

© 2019 American Meteorological Society. For information regarding reuse of this content and general copyright information, consult the [AMS Copyright Policy](https://www.ametsoc.org/PUBSReuseLicenses) (www.ametsoc.org/PUBSReuseLicenses).

and theoretical research assessing the extratropical QLCS since the 1980s. The rise and breadth of this work stems from increasingly better remote sensing of these events, as well as the development of high-resolution modeling of these and other storm types. Through these extensive research efforts [cf. Wakimoto (2001), Markowski and Richardson (2010), Trapp (2013), and Houze (2018) for overviews], we now understand that the QLCS is a distinct threat to life and property via the hazards it produces and that the QLCS poses significant operational and forecast challenges (Brotzge et al. 2013).

By using image classification and machine learning techniques on an unprecedented 22 years of composite radar reflectivity data stretching from 1996 to 2017, this research develops and employs an automated QLCS classification system to investigate the spatiotemporal characteristics of these events and their hazards across the United States. Such baseline detection and climatological work provides a fundamental understanding of where and when these events occur, an assessment of their contribution to the overall convective hazard landscape, and encourages continued efforts into understanding all aspects of the QLCS. This study is an extension of recent efforts that built a long-term, continuous United States (CONUS) hydroclimatology of extratropical MCSs (Haberlie and Ashley 2019) using image classification and machine learning approaches (Haberlie and Ashley 2018a,b). Our research also builds on earlier works that have assessed QLCSs, but over shorter periods of study or over smaller, regional domains (e.g., Parker and Johnson 2000; Burke and Schultz 2004; Trapp et al. 2005; Gallus et al. 2008; Duda and Gallus 2010), or that have produced longer, but subjective, assessments of the systems using tornado and significant severe thunderstorm report-based detection of morphologies (e.g., Smith et al. 2012, 2013; Thompson et al. 2012, 2013; Anderson-Frey et al. 2016). This study affirms some of the findings from these earlier efforts, while offering new discoveries and advancing a different methodological detection template to provide a robust and systematic capturing of these events—whether for operational or research purposes.

2. Methodology

a. Difficulties in delineating MCSs and QLCSs

For the purposes of this extratropical-based research, an MCS is defined as an assemblage of convective (i.e., ≥ 40 dBZ) cells identified in composite radar reflectivity mosaics that persists for at least 3 h and contains a contiguous or semicontiguous convective area of at least

100 km along the system's major axis (Parker and Johnson 2000; Houze 2004; Haberlie and Ashley 2019). This definition was established through the dynamical reasoning presented by Parker and Johnson (2000)—that is, the cumulative effects of convective cells interacting on scales of 100 km or greater begin to force mesoscale circulations and features after a few hours (Haberlie and Ashley 2018a,c, 2019). The Parker and Johnson criteria are the foundation to many articles that have investigated MCSs (e.g., Cohen et al. 2007; Gallus et al. 2008; Hane et al. 2008; Coniglio et al. 2010; Haberlie and Ashley 2018a,b,c, 2019).

The QLCS is a well-recognized, important, and unique subset of the wide-ranging MCS classification (Fig. 1). Convective classification schemes have matured over the decades, though, definitions of the QLCS form, which have been based on radar reflectivity imagery, have consistently been subjective, vague, and/or inconsistent, especially in their implementation. During the 1980s, QLCSs were known largely as squall lines (Bluestein and Jain 1985) or bow echoes (Fujita 1978). Though Bluestein and Jain (1985) is one of the most cited papers in the MCS literature and was one of the first to explore system taxonomy from a radar perspective, the article did not provide explicit criteria for defining these events and their subtypes. Generally, the term squall line has been replaced by the more encompassing QLCS, which was nomenclature first employed by Weisman and Davis (1998); conversely, the bow echo is still used operationally and in research to describe the “bowing out” of thunderstorms along a system's leading edge due to internal thermodynamic and kinematic processes (Fujita 1978; Przybylinski 1995). The lack of objective criteria in defining these morphologies, especially for early periods in the literature, is likely due to the insufficient quality of remote sensing facilities and networks at the time of study, as well as the bewildering spectrum of MCS and MCS subtypes that makes “binning” and classifying these events difficult and time-consuming even with high-quality, remotely sensed data. Simply, nature is complex and often rebuffs “binning” or simple one-dimensional classification systems (LaDue and LaDue 2008), but classification is necessary for developing our understanding and application of that understanding of the phenomenon studied (Doswell and Burgess 1988).

Classification of possible QLCSs can be particularly complex when linear-oriented systems are constituted by semidiscrete cells that contain stratiform precipitation linking the cells in a line. As an MCS initiates, cells may develop simultaneously while remaining relatively isolated from each other. Lines may result when these discrete cells combine and grow upscale due to cold pools

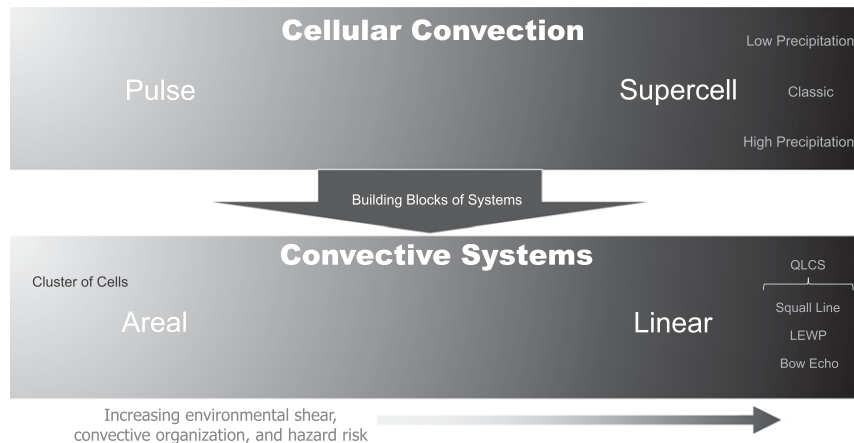


FIG. 1. Dual spectrums revealing the archetypal structures of deep, moist convection. As discussed in Doswell (2001), relatively small-scale cells (top spectrum) are the building blocks of larger convective systems (bottom spectrum). As environmental shear increases, convective organization and severe storm hazard (i.e., hail, tornadoes, and wind) risk increase.

(Weisman 1992; Weisman and Rotunno 2004) or frontal or external boundary forcing, forming a contiguous convective line (Gallus et al. 2008; Grams et al. 2012; Smith et al. 2012); however, in other cases, these cells may remain relatively discrete, yet in close proximity, while configured in a linear fashion with or without stratiform precipitation “bridging” the cells [cf. linear hybrid in Smith et al. (2012) or cells in broken squall line in Schoen and Ashley (2011)]. Other definitional considerations and complexities include: What reflectivity threshold separates stratiform from convective? How long a contiguous or semicontiguous line must be sustained to be considered a QLCS? What amount of time a convective line must be sustained in an MCS for the event to be labeled as a QLCS? How do you count QLCSs when the systems break apart and/or two (or more) systems merge? At what point does a QLCS begin and end? These questions and other intricacies lead to confusion as to what precisely constitutes a QLCS, and, therefore, how to objectively define these occurrences. Due to these difficulties, we recommend and employ an algorithm that is initially informed by basic QLCS criteria as defined in the literature and the assessments of the authors (and input from others listed in acknowledgments) that have decades of collective experience assessing MCSs and their subtypes using radar imagery. Thereafter, using specific thresholds, QLCSs may be systematically segmented, classified, and tracked using automated methods. Automated methods are requisite due to the large number of radar mosaics ($\sim 8 \times 10^5$) needed to assess in a study spanning over two decades and an area over 5×10^6 km².

b. Development of a QLCS identification and tracking algorithm

QLCSs were classified initially using the methods outlined in Haberlie and Ashley (2018c; also, cf. 2018c supplement)¹ and following the definitions espoused by Parker and Johnson (2000), Trapp et al. (2005), Gallus et al. (2008), and Grams et al. (2012). Using radar reflectivity imagery, a QLCS is defined as an MCS that has instantaneous convective (≥ 40 dBZ) regions that are longer than 100 km and must be at least 3 times as long as they are wide. In our detection of these events, we use the ~ 2 -km, 15-min resolution National Operational Weather Radar (NOWrad) dataset, which comprises quality-controlled mosaics of composite reflectivity over the CONUS. These data have been used in numerous climatologies to detect and represent many phenomena, including MCSs (e.g., Parker and Knievel 2005; Matyas 2010; Fabry et al. 2017; Haberlie and Ashley 2018c, 2019).

First, MCS events are identified in the NOWrad mosaics using image segmentation and machine learning approaches as demonstrated in Haberlie and Ashley (2018a,b). The image segmentation process aggregates convective pixels (≥ 40 dBZ) within 6 km of each other into contiguous regions, and those regions that have a major axis length of 100 km or greater are attached to surrounding stratiform (≥ 20 dBZ) precipitation within 48 km (*slices*). The machine learning process then assigns a probabilistic classification based on how closely the

¹ <https://rmets.onlinelibrary.wiley.com/action/downloadSupplement?doi=10.1002%2Fjoc.5880&file=joc5880-sup-0001-AppendixS1.docx>.

attributes of each slice agree with those of thousands of manually identified MCS and non-MCS samples (Haberlie and Ashley 2018a). To minimize the number of false positives (tropical storms, comma-heads, bright bands, and frontogenesis-induced precipitation bands produced by synoptic systems, etc.), only those slices with an MCS probability of 0.95 or greater are considered initially in this study. Qualifying slices are then spatio-temporally concatenated to produce *swaths* (i.e., the footprint of a precipitation event), and the subset of swaths that last for at least 3 h are considered MCS swaths. From the population of MCS swaths, expert pattern recognition is performed on randomly selected slices for the purpose of categorization based on composite radar reflectivity appearance. The spatial structure of slices identified as a QLCS are subjectively judged as belonging to one of the following preexisting categories identified by Parker and Johnson (2000): trailing stratiform, leading stratiform, or parallel stratiform. In contrast, non-QLCS slices are subjectively judged to belong to a nonlinear category (areal, broken, etc.; Gallus et al. 2008). Approximately 3000 slices are assigned one of two labels by the authors: QLCS (1087 samples) or non-QLCS (1835 samples). In total, 80% of these samples are used to train an image-processing, artificial intelligence system known as a convolutional neural network (CNN; Krizhevsky et al. 2012), and 20% are used to estimate the model's performance.

We use the CNN to identify QLCS (and non-QLCS) events from the overall MCS population. A CNN is used because it produces better accuracy than more traditional machine learning approaches for the image classification application used in this study (Haberlie and Ashley 2018c). The model was trained by extracting pixels in a 256 km \times 256 km region centered around the most intense portion of the sample slices. During the training process, data augmentation (Krizhevsky et al. 2012; Dieleman et al. 2015) is performed by randomly applying slight modifications to the training images to improve model generalization (translations, rotations, etc.; Krizhevsky et al. 2012). After the CNN is trained with the augmented data, it agrees with the testing data 96% of the time for non-QLCS slices and 87% of the time for QLCS slices. Further inspection of these results indicates the model may be somewhat undercounting QLCSs, as 9% of non-QLCS slices were labeled as QLCSs, but 13% of QLCS slices were labeled as non-QLCSs. Subjectively, the classifier was found to produce reasonable results, as samples with a QLCS probability of ≥ 0.95 tended to contain linear structures, while samples with a QLCS probability of ≤ 0.05 were generally nonlinear MCS structures (Haberlie and Ashley 2018c). Using the predictions from this model, MCS swaths were

considered QLCS swaths when their slices are assigned a QLCS probability of 0.95 at least once during two consecutive hourly periods (Gallus et al. 2008; Haberlie and Ashley 2018c). The methods described are used to identify QLCSs—such as in Fig. 2—in hundreds of thousands of instantaneous radar depictions, removing the subjective and laborious activity required in the past by researchers. Admittedly, our methods are likely conservative (i.e., we may “miss” smaller QLCS-like events due to relatively high standards affiliated with segmentation and classification in our methods; cf. Haberlie and Ashley (2019) section 4 discussion to this point) when delimitating QLCSs compared to others, at least as discussed and illustrated in the literature [cf. Smith et al. (2012) their Fig. 3a and Klimowski et al. (2003)'s section 2b]. Additionally, we rely solely on radar reflectivity data, so any storm mode that requires additional data (e.g., velocity couplets denoting embedded mesocyclones and, thus, potential supercells) may not be identified.

Like Haberlie and Ashley (2019), QLCS occurrences are calculated on a map by counting the number of algorithm-determined QLCS swaths that overlap a pixel location (2 km \times 2 km). Due to the sparse radar coverage and beam blockage issues that plague the WSR-88D network west of the Continental Divide, we focus on event detection in CONUS regions east of the Divide.

c. *Attributing severe thunderstorm reports to QLCSs*

To attribute severe storm reports to QLCSs, we merge the QLCS slice information developed from our algorithm with reports from the Storm Prediction Center's GIS-ready, severe report database (SVRGIS; <http://www.spc.noaa.gov/gis/svrgis>). We make no adjustments for the quality and reliability, or lack thereof, in the recorded storm data. We invite the reader to consider and recognize the assorted biases and nonmeteorological issues that have been described in the literature (cf. Kelly et al. 1985; Weiss et al. 2002; Doswell et al. 2005; Trapp et al. 2006; Brooks and Dotzek 2007; Smith et al. 2013; Strader et al. 2015; Edwards et al. 2013, 2018; etc.). It is important to note that “non-QLCS” slices may (and often do) exist within the life cycle of a QLCS swath. This is an implementation detail to improve the continuity of swaths. However, storm reports in these non-QLCS slices are not considered “QLCS” reports.

Portions of the objective attribution process employed are illustrated on a sample QLCS swath in Fig. 2. In some cases—especially with fast moving events or events with outflow that extends in advance of the precipitating line—storm reports may occur in regions with no radar reflectivity. We tested several buffers around qualifying QLCS slices to capture such events, and determined that a 20-km (~ 12 -mi) buffer around the slice [e.g., see

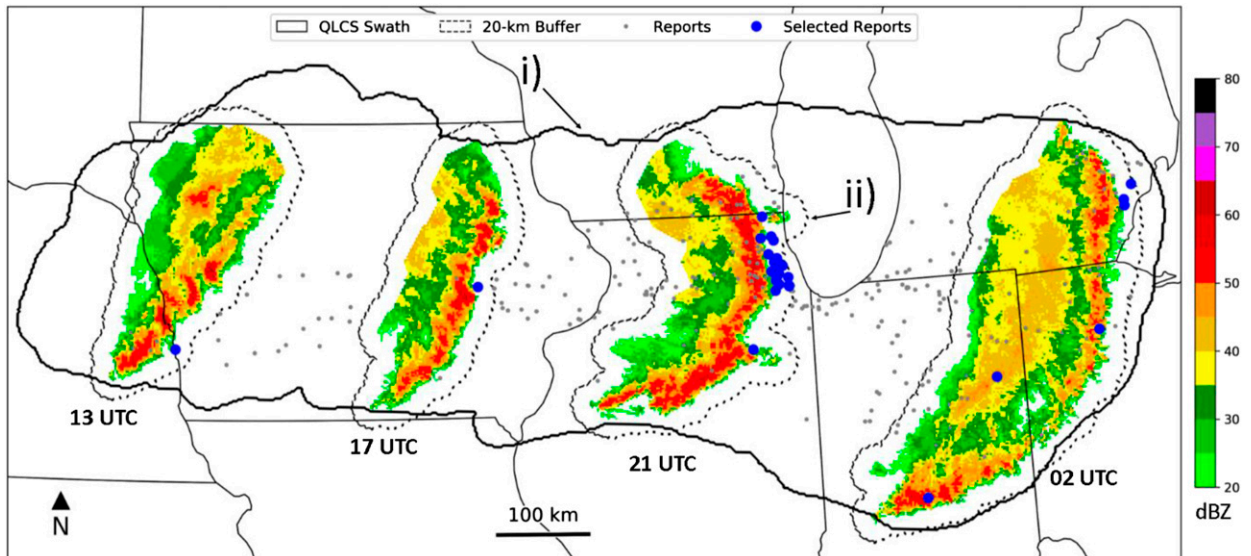


FIG. 2. An example QLCS swath (labeled i) from 1130 UTC 18 Jun 2010 to 0230 UTC 19 Jun 2010. Gray and blue dots are all the severe reports that were attributable to this QLCS swath. A visual example of the report selection process is provided for the slices that occurred, from left to right, at 1300, 1700, and 2100 UTC 18 Jun 2010 and 0200 UTC 19 Jun 2010. A 20-km buffer is generated around each QLCS slice (e.g., ii; dashed polygon) to gather reports affiliated with that slice. Any reports that meet the following criteria are denoted by the large blue dots: 1) occurred within ± 7.5 min of the corresponding slice and 2) are within the buffered region.

dashed polygon (ii) in Fig. 2] was the most effective at gathering reports that may lie ahead of the slice, while reducing the possibility of sweeping up reports due to isolated convection ahead of QLCS. Despite efforts to reduce captures of isolated cells immediately ahead of the line, the method still includes some reports due to cells, especially as cells were merging with the line (e.g., French and Parker 2012) or so-called tail-end Charlie events (Branick 1996). This false capturing, which we discuss further in section 4b, tended to occur sparingly on high-end severe days where both supercell and QLCS structures occurred in the same environmental ingredients space.

We do not differentiate between QLCSs that have embedded supercell or “classic” mesocyclone-like structures—however those may be defined—from those that do not exhibit such features (cf. Smith et al. 2012). We make no differentiation between hazards produced by so-called QLCS mesovortices (e.g., Trapp and Weisman 2003) from line-embedded, supercell-induced tornadoes, even though we acknowledge that processes that engender tornadoes in QLCSs can vary depending on the environment and mesocyclone typology. In the end, a tornado produced by a more classical mesocyclone, supercell-like structure embedded in a QLCS is still a tornado induced by a parent QLCS.

Overall, any reports that occurred within ± 7.5 min of the corresponding slice and that were within the buffered region were qualified QLCS reports. Spatial

analyses related to SVRGIS data are presented on an $80 \text{ km} \times 80 \text{ km}$ grid, which is equivalent to the SPC’s probabilistic hazard outlooks and verification products.

d. Methodology limitations

Current automated approaches to identifying MCS and QLCS events cannot match the skill of an experienced and engaged research or operational meteorologist with several datasets at their disposal. Perhaps the largest contributing factor is the well-known limitation of tracking approaches when dealing with splitting and merging events (Lakshmanan and Smith 2010). Further, Haberlie and Ashley (2018b) show examples of how the approach that is used when identifying events of interest can influence the resulting climatology of these events. These methods are also limited by the quality of the underlying data and any spatial and systematic heterogeneities included in those data (Parker and Kniefel 2005). Radar data are not immune to heterogeneities in data quality, and there are well-known issues relating to radar coverage, anomalous signals, and other considerations (Smith et al. 1996; Parker and Kniefel 2005; Fabry et al. 2017). In particular, areas with sparse radar coverage (e.g., the High Plains) are more likely to have lower detection sensitivity, as both segmentation and tracking are influenced by missing radar returns below 1800 or even 3000 m. Additionally, since this work did not consider any data beyond radar reflectivity, it is limited in the ability to detect line- or cluster-embedded

supercell structures. This is a deviation from the methods of [Smith et al. \(2012\)](#), who also considered velocity data in addition to radar reflectivity. As a result, any embedded supercell structures that can only be detected using velocity data may not be identified in this work. However, as we show, our approach still produces results that agree with previous work, with a few exceptions. The authors implore the reader to assess the results presented herein with these important caveats in mind.

Despite these problems, the strength of automated approaches is the consistent application of identification and tracking rules (however limited they may be), as well as the ability to process millions of radar images (with all the affiliated issues) in a reasonable amount of time. The tracking approach used in this paper ([Haberlie and Ashley 2018b](#)) allows a great deal of customization. Presently, a strict MCS probability and a small segmentation search radius applied to slice candidates limit the dataset to some of the most intense MCS cases. Reducing this MCS standard to include more marginal events would likely involve more hurricanes/synoptic systems/etc., particularly in the Southeast United States ([Haberlie and Ashley 2018b](#)). Thus, there is the added heuristic of lowering the sensitivity to MCS and QLCS events (i.e., fewer MCS and QLCS events included), while increasing specificity (i.e., more non-MCS and non-QLCS events disqualified).

The association of severe weather reports with radar-identified events also increases the complexity of the method. For example, even perfectly positioned severe weather reports can exist kilometers from the nearest, legitimate, radar reflectivity returns. Several search radii were tested to balance capturing events associated with QLCSs, while excluding reports that were near QLCSs, but were clearly affiliated with a different storm mode. This issue appears to be most prevalent with significant tornado events. The mixed-mode and widespread coverage of radar returns during many of these events pose a challenge to our approach. We discuss a manual inspection of these cases in [section 4b](#), as well as our interpretation of those findings. Again, we urge the reader to assess the results of this paper in the context of those stratified accuracies.

3. QLCS occurrences

a. Spatiotemporal QLCS climatology

There were 3064 QLCSs identified across the CONUS during the 22-yr study period, with a mean (median) of 139 (138) per year. The annual frequency of the events was variable with a high of 178 in 2008 and a low of 101

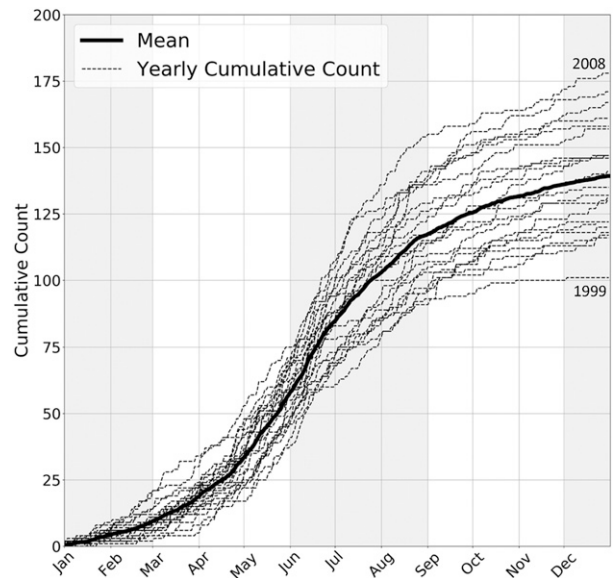


FIG. 3. Cumulative frequency diagram of the mean (bold) and individual yearly QLCS counts (dashed) from 1996 to 2017 for the CONUS. Years with the highest (2008) and lowest (1999) QLCS counts are noted.

in 1999 ([Fig. 3](#)), with the variability driven largely by late spring and early summer QLCS populations ([Fig. 4](#)). A linear least squares fit reveals a small increase in the number events during the period ($+0.5 \text{ yr}^{-1}$), but, due to the short period of record, it is difficult to discern the significance of this trend. Despite the increasing trend, four of the five lowest QLCS count years are during the latter period of record—from 2012 to 2015.

QLCSs occur primarily in the central and eastern CONUS ([Fig. 5a](#)). There may be cases in the western CONUS (e.g., [Ladue 2002](#); [Corfidi et al. 2016b](#)) that our methodology did not capture, but this absence is due to insufficient radar coverage—requisite for our algorithm—west of and along the Continental Divide, as well as in the High Plains (cf. [Fig. A1](#) in [Parker and Knievel 2005](#)). There are two distinct QLCS maxima ($>16 \text{ QLCS yr}^{-1}$) over the central CONUS: 1) far eastern Great Plains and western Ozark Plateau and 2) central Mississippi and western Tennessee River Valleys. Broadly, the central and eastern CONUS contains a climatological prevalence of ingredients—lower-tropospheric moisture, CAPE, adequate shear, continual thermal forcing, and the existence of other features (e.g., shortwave troughs, extratropical cyclones and their fronts, nocturnal boundary layer wind maxima, drylines)—that are supportive of thunderstorms that can initiate and grow upscale into MCS structures, including QLCSs ([Johns and Doswell 1992](#); [McNulty 1995](#); [Carbone et al. 2002](#); [Parker and](#)

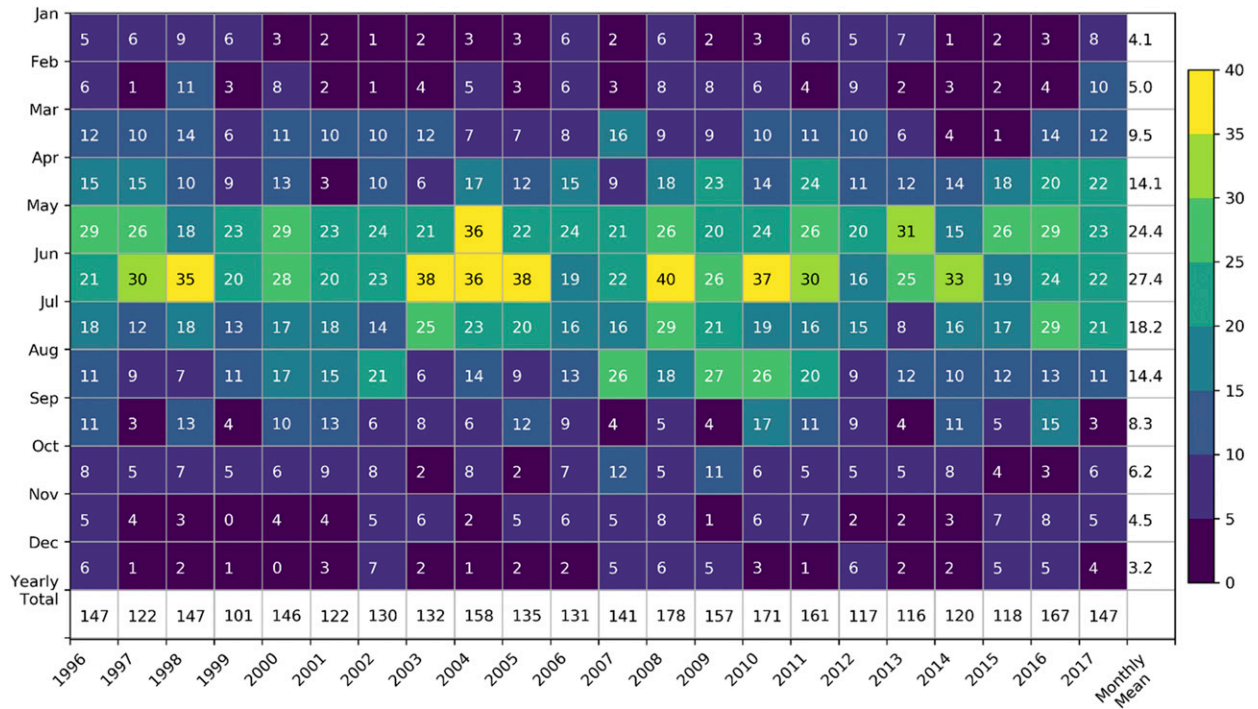


FIG. 4. Total yearly (bottom row) and monthly QLCS counts (grid cells), as well as monthly mean QLCS counts (far right column), from 1996 to 2017 for the CONUS.

Ahijevych 2007; Cohen et al. 2007; Trier et al. 2010; Gensini and Ashley 2011). The east-central Great Plains and western Ozark maximum is, at least in part, due to diurnally forced convection that initiates in the High Plains and the Rocky Mountains owing to, for example, terrain, dryline, or frontal forcing. As this convection moves east due to the westerlies, it can grow upscale and

mature into intense systems that are sustained by migrating extratropical systems (Whittaker and Horn 1984; Eichler and Higgins 2006), the nocturnal boundary layer wind maximum (Higgins et al. 1997; Kumjian et al. 2006; Coniglio et al. 2010), and/or internal processes such as the formation of cold pools and gravity currents (Carbone et al. 2002; Trier et al. 2010).

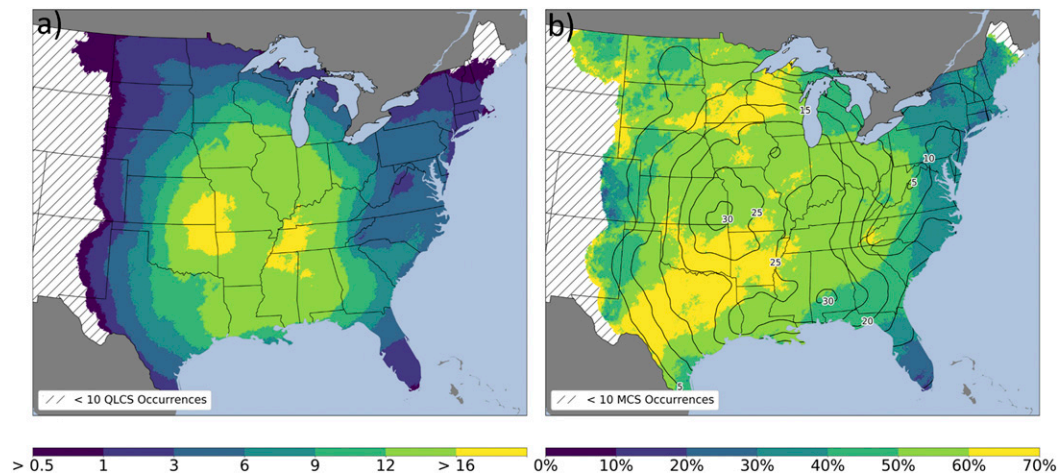


FIG. 5. (a) Mean annual QLCS swath occurrence and (b) proportion of MCSs that are QLCSs (shaded) and mean annual MCS swath occurrence (solid contours) from 1996 to 2017. Occurrences and percentages are calculated on a 2 km × 2 km grid.

The central Mississippi and western Tennessee River Valleys maximum is due to a combination of factors and, moreover, a relatively frequent overlap of environments supportive of QLCS formation and sustenance. First, as extratropical cyclones develop and mature east of the Rocky Mountains, they produce maxima in convection in phases coincident with the diurnal cycle and their migration due to the westerlies across the central and eastern CONUS (Carbone et al. 2002). Convective phases in extratropical cyclones can include diurnally forced convection as the cyclone and affiliated upper-level trough first encounters moisture and instability along the western edge of the Great Plains and, during the next day, a second phase of convection as instability increases in the warm sector of the extratropical cyclone due to diurnally driven insolation and surface heating. These situations can spur multiday episodes of severe weather across the CONUS (Ashley et al. 2005, 2007; Shafer and Doswell 2011). Additionally, Carbone et al. (2002) discovered coherent, warm-season precipitation signals across the CONUS, including the central Mississippi and western Tennessee River Valleys region, that were made up of successive MCSs that appeared to be forced by convectively generated mechanisms such as trapped wavelike disturbances or, possibly, mesoscale convective vortices (MCVs; e.g., Trier and Davis 2007). In comparison to other regions (e.g., Great Lakes, Great Plains, Southeast), the central Mississippi and western Tennessee River Valleys region has a much longer environmental period during the year where ingredients necessary for the formation and sustenance of systems may be juxtaposed. For instance, the region is affected by high-shear, low-CAPE environments supportive of QLCSs during the cool season (Burke and Schultz 2004; Sherburn and Parker 2014; Sherburn et al. 2016), migratory extratropical cyclones and their fronts and prefrontal troughs during the cool and transition seasons (Whittaker and Horn 1984; Eichler and Higgins 2006; Bengtsson et al. 2006; Lukens et al. 2018) that can externally force QLCSs (Newton 1950; Stoelinga et al. 2003), and a wide spectrum of environments during the warm season that can be supportive of upscale growth due to system-internal forcing, such as cold pools (Johns 1984; Stensrud and Fritsch 1993; Coniglio et al. 2004; Guastini and Bosart 2016).

Seasonally, the frequency of QLCSs increases appreciably in March (Fig. 4) with a spatial count maximum in the mid-South (Fig. 6) and peaks during the warm season in June across the Great Plains and Midwest. On average, over 27 QLCS events occur in June, with six of the seven most active months during the 22-yr climatology during this month. The latter part of the warm season—July and August—has notably fewer QLCS counts than May and June. The roughly 30% drop in

QLCS counts from June to July may be a result of reduced baroclinity and traveling extratropical cyclones that occur during the mid and latter part of the warm season as the westerlies shift poleward toward and, eventually, into Canada (Rudeva and Gulev 2007; Belmecheri et al. 2017). In addition, a smaller region of the CONUS is supportive of organized convection and its sustenance during the latter warm season due to increasing capping strength under a seasonal anticyclone often anchored in the south or southwest CONUS (Galarneau et al. 2008; Myoung and Nielsen-Gammon 2010a,b,c; Ribeiro and Bosart 2018). This thrusts the primary corridor of QLCSs into the Corn Belt and Upper Midwest during July and August, as poleward-directed, instability “underrunning” (Doswell and Bosart 2001) commences beneath the ridge and mesoscale, upper-level, potential vorticity disturbances—known as “ridge rollers”—can initiate and sustain convective systems (Bosart et al. 1999; Galarneau and Bosart 2006; Wang et al. 2011). This warm-season, high-occurrence corridor is frequented by northwest flow (NWFL) severe weather outbreaks and other synoptic patterns that can produce QLCSs (Johns 1982, 1984; Wang et al. 2011; Guastini and Bosart 2016; Pokharel et al. 2019) and progressive derechos that, by contemporary definitions, are produced by linear systems (Coniglio and Stensrud 2004; Guastini and Bosart 2016; Corfidi et al. 2016a). After September, QLCSs become relatively infrequent until spring, averaging around, or, in most cases, less than, five per month during the cool season. Events during this season are confined largely to the mid-South and Gulf Coast, where limited, but sometimes sufficient, moisture can coincide with forcing due to migratory extratropical cyclones to generate long-lived, linear morphologies (Geerts 1998; Parker and Ahijevych 2007). In some cases, these cool-season cyclones generate high-shear, low-CAPE environments supportive of QLCSs that produce hazards that are operationally difficult to detect and warn (Thompson et al. 2012; Smith et al. 2012; Brotzge et al. 2013; Sherburn et al. 2016; Anderson-Frey et al. 2016). As with the broader MCS classification (Schumacher and Johnson 2006; Carbone and Tuttle 2008; Haberlie and Ashley 2019), QLCSs exhibit a distinct diurnal pattern, tending to initiate in the late afternoon and evening hours (Fig. 7a) and dissipate near sunrise (Fig. 7b).

b. MCSs and the QLCS subclassification

On average, 32% of MCSs are QLCSs; uniquely, there is not much variation in this proportion over the study period, with the percentage of MCSs that are QLCSs within 29% and 38% in any given year (Fig. 7c). The proportion of MCSs that are QLCSs does decline over the year, from a broad maximum of 30%–40% of MCSs

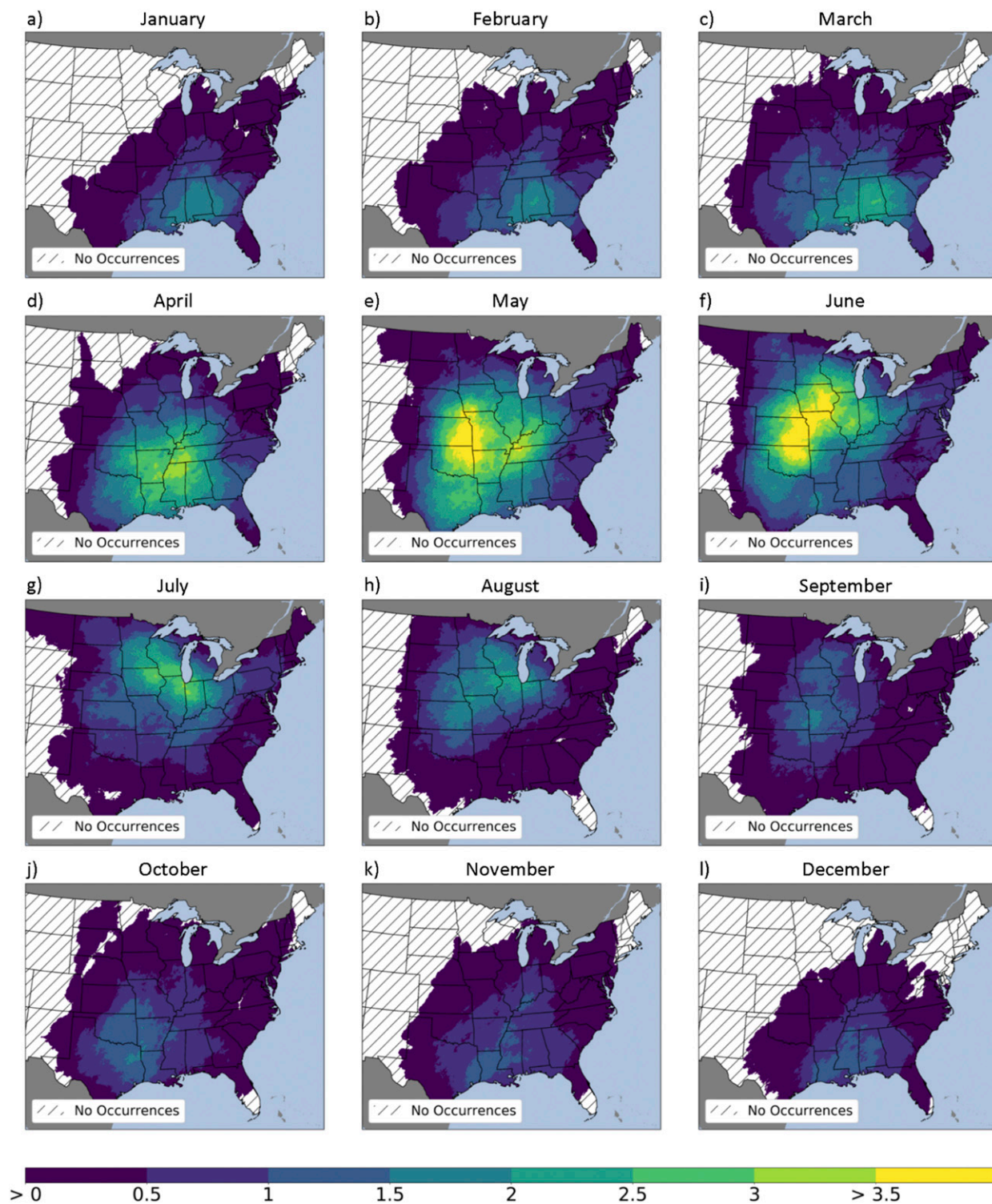


FIG. 6. As in Fig. 5a, but for mean monthly QLCS counts.

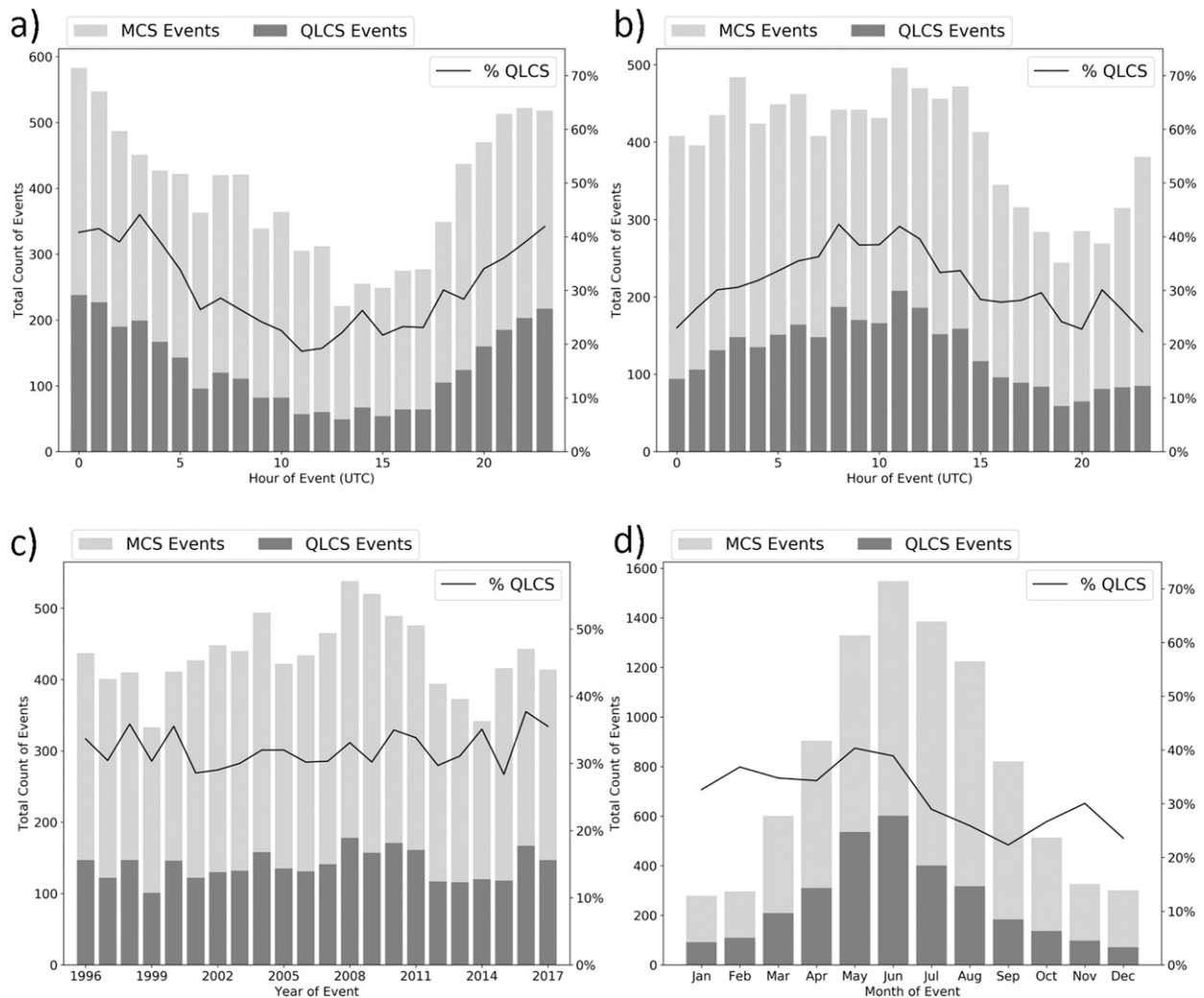


FIG. 7. Counts and percentage of MCSs that are QLCSs for the following temporal attributes: (a) initiation by hour, (b) termination by hour, (c) annual, and (d) monthly.

from January to June to a minimum of just over 20% in September and December (Fig. 7d). MCS populations do not have as dramatic a decline in numbers from June to July as was illustrated with QLCSs; indeed, the MCS population seasonal peak is much broader and shifted to later in the warm season, including relatively high counts in both July and August. This suggests that highly organized MCS structures tend to wane during the latter warm season, whereas less-organized, nonlinear MCSs, such as back-building and areal forms, become more commonplace. Declining baroclinity and resultant weakening of low- and deep-layer shear (cf. Fig. 2 in Gensini and Ashley 2011), ingredients often necessary for linear structures (Weisman and Rotunno 2004; Coniglio et al. 2006), is at least one reason for the reduced frequency of QLCSs during this latter warm-season period, which otherwise features abundant instability (cf. Fig. 3 in

Gensini and Ashley 2011). Diurnally, the proportion of MCSs that are QLCSs is greatest during the late evening and overnight hours (Figs. 7a,b), which may be, in part, due to increasing low-level shear found during the nocturnal period in many areas of the central CONUS due to the low-level jet (Shapiro et al. 2016; Geerts et al. 2017); this nocturnal shear is important for system organization and sustenance (French and Parker 2010; Blake et al. 2017).

Broadly, MCSs (Fig. 5b) and the MCS subclassification, QLCS (Fig. 5a), have similar spatial patterns of occurrence. The proportion of MCSs that are QLCSs is greater than 50% for large expanses of the central CONUS (Fig. 5b), with two broad maxima (60%–70%) found throughout Upper Midwest (Minnesota and Wisconsin) and in the southern and south-central Great Plains (Arizona, Oklahoma, and Texas). Seasonally (not shown),

these percentages peak near 80% in the southern Great Plains and Arklatex regions in the spring, portions of the Midwest in the summer, and the southern Appalachians in the winter.

4. QLCS-attributable severe thunderstorm reports

There is an extensive body of literature that has implicated the QLCS—or equivalent in other parlance (e.g., squall line, bow echo, etc.)—as a source for severe thunderstorm hazards, most notably tornadoes and damaging winds. Much of this literature is summarized by Trapp et al. (2005) for tornadoes, and Wakimoto (2001) for nontornadic winds. Trapp et al. (2005) were the first to systematically approach the question of how many tornadoes are produced by linear system morphologies, as the scientific focus during the latter twentieth century had trended to supercells; though, this focus was certainly justifiable as supercells produce most strong-to-violent tornadoes (Smith et al. 2012) and supercell-related tornadoes are responsible for over 90% of tornado deaths in the CONUS (Schoen and Ashley 2011; Brotzge et al. 2013). QLCS-related hazards, especially tornadoes, are being detected with increasing efficiency due to many reasons, including: recent superresolution, polarimetric, and sampling improvements to the WSR-88D network (Kumjian 2013; Chrisman 2014; Thompson et al. 2017); the dissemination and operational use of Terminal Doppler Weather Radar in NWS offices (Vasiloff 2001); awareness and results from field campaigns, as well as observational and numerical modeling studies, assessing mesovortices in QLCSs (e.g., Trapp and Weisman 2003; Atkins et al. 2005; Trier and Davis 2007); emphasis on training forecasters to anticipate QLCS mesovortexgenesis (e.g., Schaumann and Przybylinski 2012); and improvements in postevent surveying, including dissemination and assessments of very high-resolution aerial and satellite imagery of postevent landscapes (e.g., Skow and Cogil 2017). Complexity remains in identifying whether some of the circulations found on radar and narrow damage tracks uncovered posthumously are produced by tornadoes or low-level meso- γ -scale vortices, such as those described in Trapp and Weisman (2003), Schenkman et al. (2012), and Flournoy and Coniglio (2019). These hazard-inducing circulations can be embedded within a broader region of nontornadic, “straight-line” winds that produce equivalent damage (e.g., Atkins et al. 2005; Wakimoto et al. 2006; Schenkman and Xue 2016), making hazard delineation difficult, especially for those postevent assessments with limited damage indicators or resources. Simply, where exactly the cutoff is for what constitutes tornadic damage is often difficult and is scenario- and opinion-dependent, even in

high-end, tornadic supercell cases (Wurman et al. 2014; Wakimoto et al. 2016).

In this section, we employ the historical severe thunderstorm report record in conjunction with the QLCS detection and tracking algorithm to estimate the amount, proportion, and spatiotemporal attributes of severe and significant severe hazards produced by QLCSs for the 22-yr period of record. We restrict our analysis to a large domain most frequented by QLCSs, which is a domain well sampled by radar. In addition, we eliminated a small proportion of storm reports from consideration in this domain since there was no corresponding radar imagery at the time of a report, making morphology attribution difficult. Overall, 93.4% (95.9%) of the storm reports in the CONUS (storm report study domain) database are sampled using this method.

a. QLCS severe thunderstorm hazard occurrence

Nearly 20% of severe thunderstorm reports in the central and eastern CONUS are produced by QLCSs (Table 1). The proportion of storm reports due to QLCSs is highest in the Mississippi, Ohio, and Tennessee River Valleys, with over 40% of storm reports in the lower Ohio River Valley due to this morphology (Fig. 8a). Seasonally, the proportion of QLCS-severe storm reports is highest from October through March, with more than 40% of reports due to QLCSs in November, January, and February. Spatially, the proportion of QLCS storm reports is highest in the winter, with large expanses of the southern Great Plains, Ohio River Valley, Southeast, and mid-Atlantic with over 40%—to as high as 82%—of their storm reports due to QLCSs (Fig. 9). The QLCS-attributable proportion drops to a minimum for the domain during the warm season, with less than 15% of reports due to QLCS in July, August, and September; this relatively low proportion is due to the prevalence of unorganized convection during this period for large expanses of the domain (Miller and Mote 2017). However, QLCS hazards constitute well over 30% of all storm reports in many areas of the Midwest and Corn Belt during the warm season.

Nearly 85% of QLCSs produce at least one severe thunderstorm report, with over 50% (10%) of events producing 10 (100) reports or more (Fig. 10). There have been five events that have yielded over 600 reports including 4–5 April 2011 (1163 reports), 29–30 June 2012 (788), 6–7 March 2017 (684), 19–20 April 2011 (658), and 1 March 2017 (627).

b. QLCS tornado occurrence

Roughly 21% of reported tornadoes are attributable to QLCSs during the 22-yr study period (Fig. 11a). In a 3-yr investigation from 1998 to 2000, Trapp et al. (2005)

TABLE 1. The number of monthly and total severe thunderstorm reports by hazard, as well as the proportion of those reports attributable to QLCSs for the 22-yr period as delineated using the spatiotemporal methods outlined in section 2c. Reports are those from SVRGIS within the analysis domain (cf. interior rectangle in Fig. 8 panels) and where radar data were available at time of report. Boldface cells denote highest value for each attribute.

Month	All severe reports			Tornado			Severe wind			Severe hail		
	Reports	QLCS reports	QLCS %	Reports	QLCS reports	QLCS %	Reports	QLCS reports	QLCS %	Reports	QLCS reports	QLCS %
Jan	8091	3335	41%	801	358	45%	4935	2322	47%	2355	655	28%
Feb	11 362	5032	44%	754	311	41%	6411	3725	58%	4197	973	23%
Mar	31 818	8414	26%	1726	493	29%	10 704	4931	46%	19 388	2877	15%
Apr	65 454	14 947	23%	3861	1046	27%	21 510	8652	40%	40 083	4980	12%
May	10 4349	20 787	20%	5739	1130	20%	39 230	13 228	34%	59 380	5959	10%
Jun	123 364	24 035	19%	4172	638	15%	65 902	18 470	28%	53 290	4418	8%
Jul	93 887	13 110	14%	2131	236	11%	61 757	11 304	18%	29 999	1340	4%
Aug	58 619	5827	10%	1440	113	8%	36 166	4733	13%	21 013	891	4%
Sep	23 116	3471	15%	1338	65	5%	12 388	2648	21%	9390	686	7%
Oct	13 371	3452	26%	1198	232	19%	7089	2614	37%	5084	553	11%
Nov	9371	3799	41%	1166	344	30%	5958	2813	47%	2247	589	26%
Dec	5407	1895	35%	612	188	31%	3412	1399	41%	1383	299	22%
Total	548 209	108 104	20%	24 938	5154	21%	275 462	76 839	28%	247 809	24 220	10%

found that 18% of tornadoes were produced by QLCSs. Our proportion of QLCS tornadoes (17.3%) is equivalent to Trapp et al.'s finding during the overlapping three years, adding confidence to the automated methods embraced in this research. There is also a notable increase in the proportion of QLCS tornadoes since 2008, with proportional peaks in 2011, 2013, and 2017 at 34.6%, 35.0%, and 38.9%, respectively. Although there is some uncertainty related to nonmeteorological factors, including those in reporting, we postulate that the larger proportion of QLCS tornadoes found in the latter third of the record (~29.1% from 2011 to 2017) is more climatologically representative due to better understanding and documentation; however, additional years of data will be required to confirm this hypothesis. Direct comparison of our output with Smith et al.'s (2012) relative storm report attribution frequency is difficult due to differing methodologies and periods of analysis. That said, their relative frequency of QLCS tornadoes is near 14%, whereas their more encompassing "linear" morphology, which includes QLCSs, right-moving supercell in line, and line marginal modes, is responsible for over 25% of their relative counts. These values are comparable with our proportions, despite different methodologies and study periods. It should be noted that the necessity of including the numbers from "right-moving supercell in line" to produce comparable proportions affirm Smith et al.'s (2012) findings that linear modes identified only by patterns in radar reflectivity might belie the true nature of embedded updrafts. Although one should hesitate to discount a supercellular origin for the reports identified as QLCS events in this work, the overarching

theme of complex, widespread, and linearly organized convection associated (at least spatially) with significant and even violent tornadoes remains consistent with findings in the literature.

Initially, the proportion of QLCS-attributable tornadoes increases as the EF scale increases, jumping from 21% of all tornadoes, to 29% of EF1+ and 26% of EF2+ (Table 2). As espoused by Trapp et al. (2005), a non-negligible proportion of weak QLCS tornadoes may go unreported, though we postulate, as suggested above, that advances in the WSR-88D network and postevent assessments have reduced this undocumented proportion during the period. The QLCS proportion decreases as prescribed damage intensity moves into intense (EF3+) and violent (EF4+) events, with those EF-scale thresholds accounting for 20% and 15%, respectively. There have been no documented EF5s associated with QLCSs. Though difficult to compare directly our results with Smith et al. (2012), our proportions are generally within the range of percentages Smith et al. produced for QLCSs and their more encompassing "linear" morphology, especially for EF0+ through EF2+ events. We do differ, and have higher QLCS contributions, for EF3+ and EF4+.

The initially perceived unique proportional contributions from QLCSs found for strong tornadoes prompted additional testing. As we discuss at the conclusion of section 2, the image segmentation, bridging, and 20-km buffering methodology may permit, in some cases, false capturing of isolated, mesocyclone-induced tornadoes due to supercells and ascribing those events as QLCSs. To test, we manually classified over 3100 algorithm-identified QLCS tornadoes from 2007 to 2017, placing

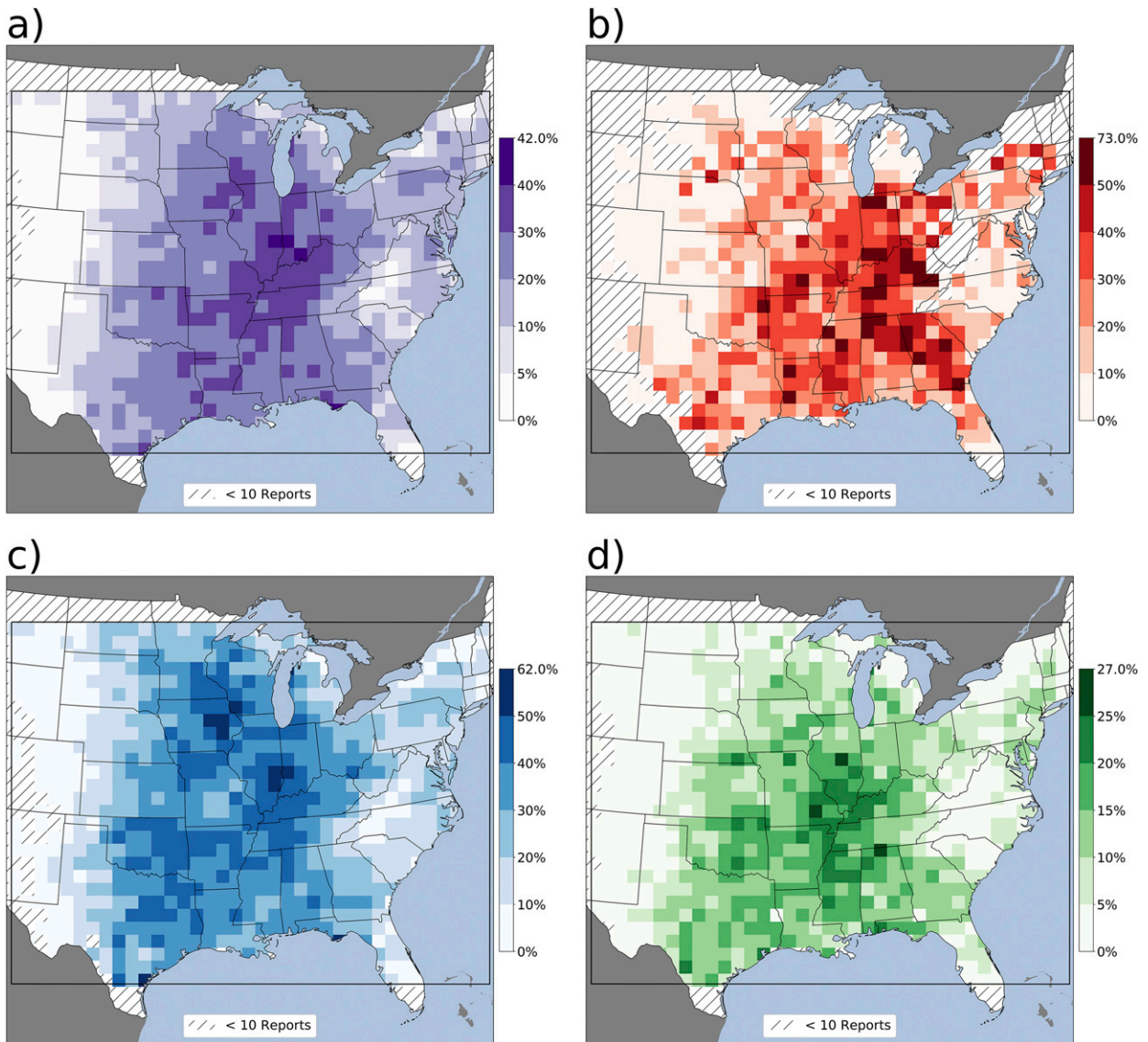


FIG. 8. The percent of (a) all severe thunderstorm hazards, (b) tornadoes, (c) nontornadoic severe wind, and (d) severe hail reported in an 80 km \times 80 km grid cell due to QLCS structures. Only cells with ≥ 10 reports or in the study domain are filled. Severe hazard attribution study area denoted by interior rectangle in panels.

each event in one of three classes: QLCS, non-QLCS, or “undetermined”. The non-QLCS events, or false captures, were typically affiliated with isolated supercell-like structures that were visibly disconnected from the algorithm-identified QLCS, but were within the buffer region and, in some cases, likely to be swept up by the QLCS in time or, in other cases, were detached tail-end Charlie type events. These events tended to occur on high-end days where both supercell and QLCS structures occurred in the same environmental ingredients space. With the “undetermined” classification, we struggled in deciding due to stratiform or convective bridging that can occur in and around systems. Overall, the test

revealed an algorithm accuracy ranged from 89.1% to 95.4% for EF0+ events. Specifically, the 95.4% is inclusive of those labeled QLCS *and* “undetermined”, whereas the 89.1% is based solely on QLCS-labeled events, with non-QLCS *and* “undetermined” cases attributable to a 10.9% overcounting error. This error increases as the EF scale increases. The algorithm had an accuracy range of 83.1%–92.9% for EF2+, and 68.2%–87.1% for EF3+. These results show that the automated approach creates a reasonably accurate estimate of QLCS-affiliated tornado reports, but struggles with relatively rare, strong tornadoes that exist in the same environmental space as a QLCS.

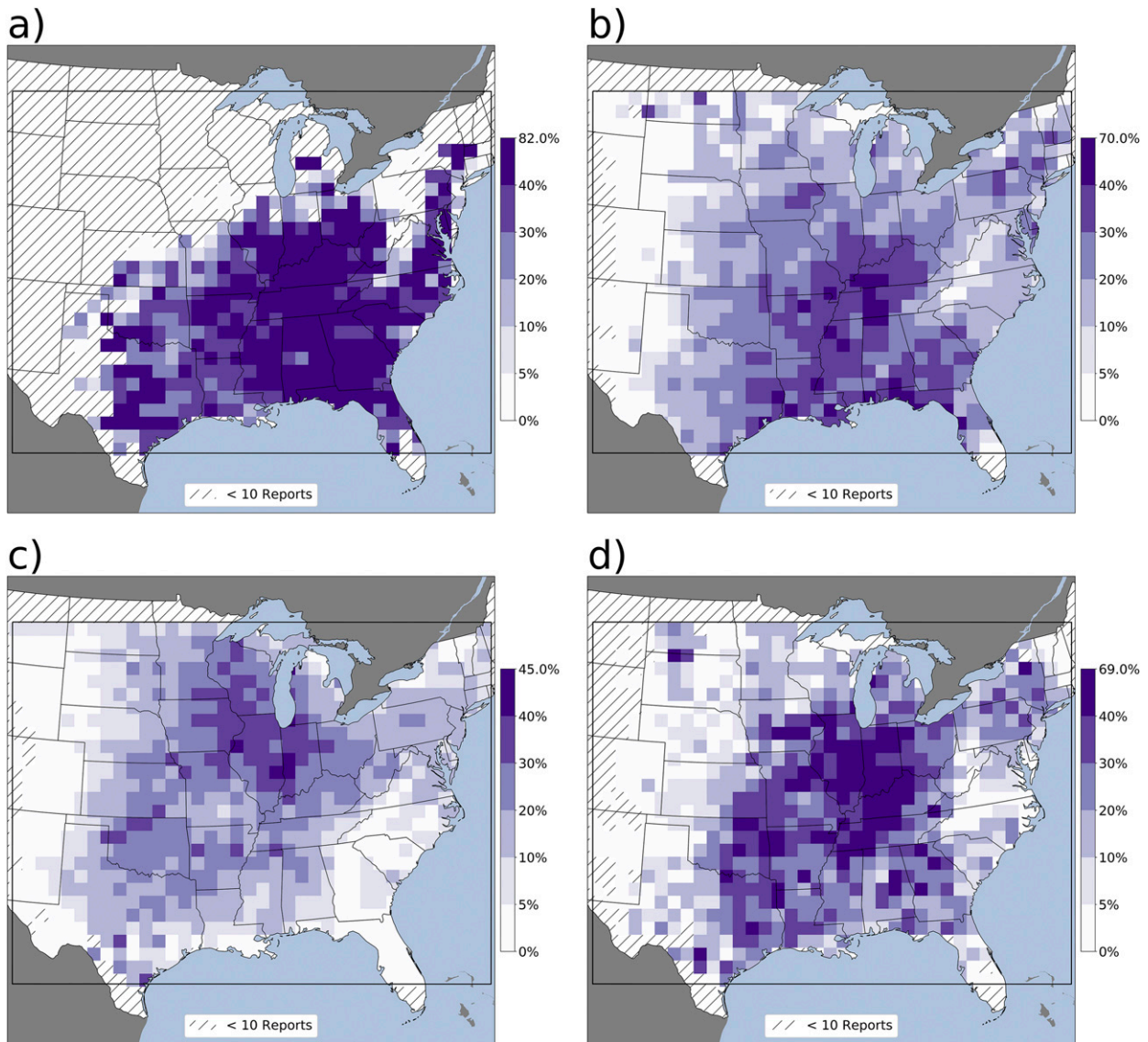


FIG. 9. The percent of all severe thunderstorm hazards reported in an 80 km \times 80 km grid cell due to QLCS structures for (a) winter (DJF), (b) spring (MAM), (c) summer (JJA), and (d) fall (SON). Only cells with ≥ 10 reports or in study domain are filled.

Seasonally, QLCS tornadoes are most frequent in April, May, and June, yet the proportion of tornadoes due to QLCSs is highest from November through March (Fig. 11b). During the period of record, the proportion of QLCS tornadoes has been increasing in all seasons over time. The most demonstrable growth was during the winter (December–February), from 31.6% for 1997–2003, to 35.2% for 2004–10, to 49% for 2011–17. The spring season (March–May) also witnessed large proportional increases, from 16.2% in the 1997–2003 period to over 33% in the latter 7 years. Interestingly, there were, on average, 6770 non-QLCS tornadoes during each of the two earlier 7-yr periods, which dropped to just over 5300 during the last 7-yr period; conversely,

there were 1263 and 1542 QLCS tornadoes during the first two 7-yr periods, respectively, which increased to 2186 QLCS tornadoes in the last period. This divergence in QLCS and non-QLCS tornado counts may be illustrative of an increasingly better understanding of the QLCS and the hazards they produce, as well as their detection and postevent assessments that accompanied many of these events in the latter period.

Spatially, the proportion of tornadoes due to QLCSs is clustered west of the Appalachians, stretching from the lower Great Lakes to the mid-South (Fig. 8b). Many grid cells in this region have over 50%—to as high as 73%—of their reported tornadoes due to the QLCS morphology. Kentucky and Indiana had the most QLCS-affiliated

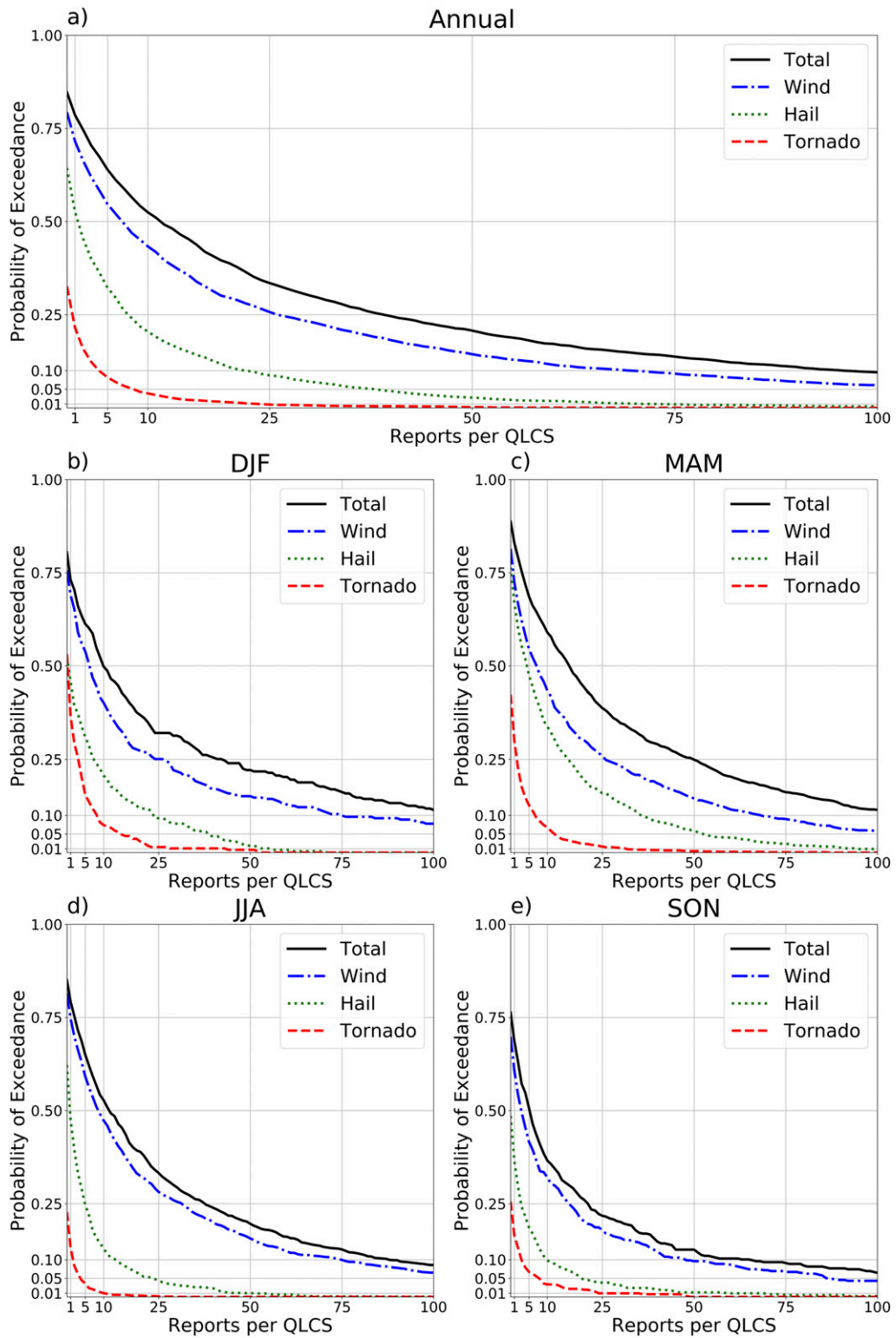


FIG. 10. Probability of exceedance curves for all severe thunderstorm reports (black; solid), tornadoes (red; dashes), severe wind (blue; dash-dots), and severe hail (green; dots) for (a) annual, (b) winter (DJF), (c) spring (MAM), (d) summer (JJA), and (e) fall (SON).

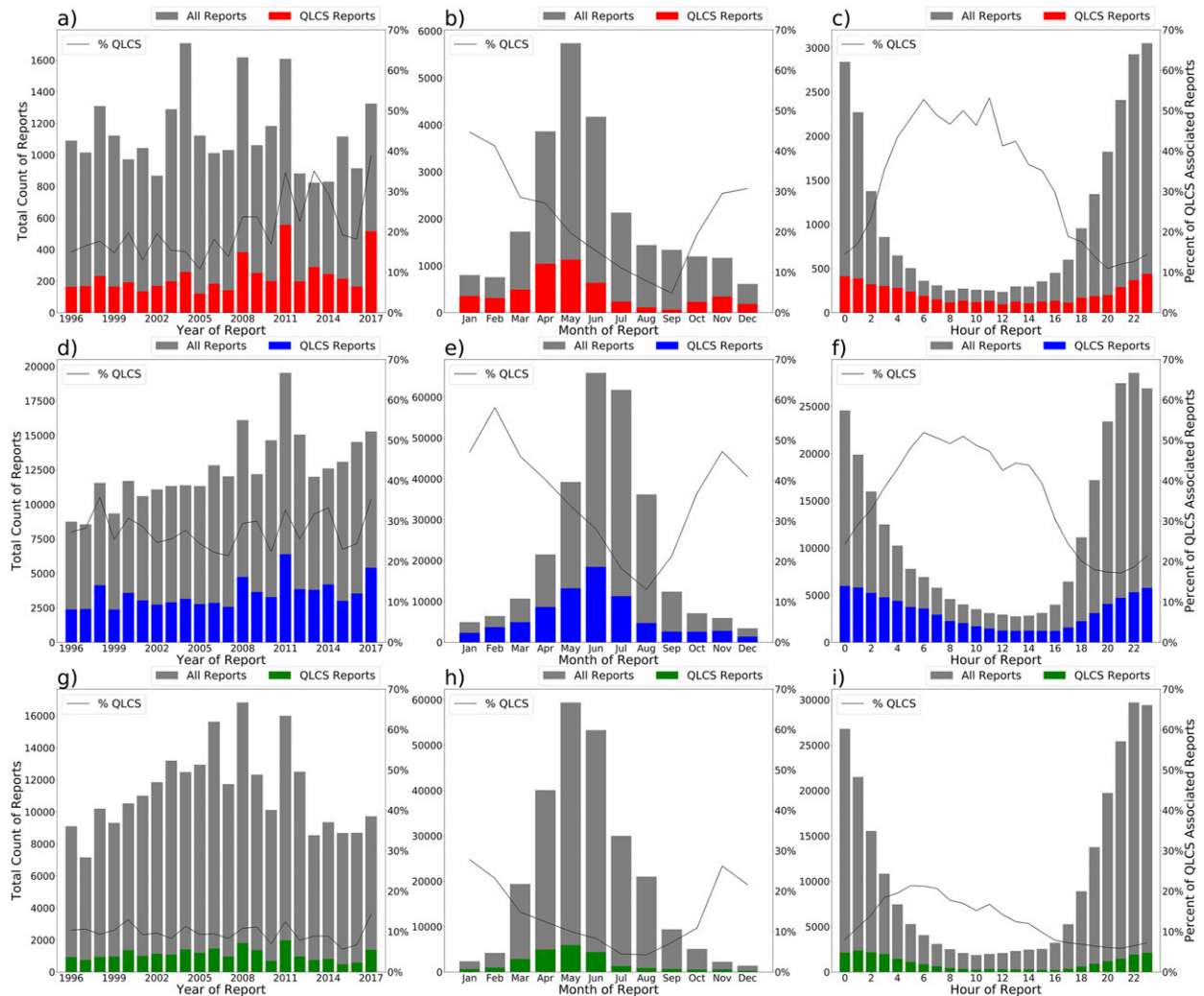


FIG. 11. (a) Annual, (b) monthly, and (c) hourly counts (left axes) and percent (right axes) of tornadoes produced by QCLSs. (d)–(f) As in (a)–(c), but for severe wind, and (g)–(i), as in (a)–(c), but for severe hail.

tornadoes with 43% and 40% of events due to this morphology, respectively. Over 35% of tornadoes in Alabama, Georgia, Mississippi, and Tennessee, and over 30% of events in Arkansas, Ohio, and Illinois are due to QCLSs. Most tornadoes are produced by QCLSs in many areas of the mid-South and central and lower Mississippi and Ohio River Valleys during the winter and spring season (Fig. 12). This region is characterized by relatively low warning performance (Anderson-Frey et al. 2016), which may be, at least in part, due to the predominance of QCLS tornadic environments, often featuring high-shear, low-CAPE ingredients (Thompson et al. 2012, 2013; Anderson-Frey et al. 2016) and, generally, shallower and weaker tornadic circulations that are difficult to detect (Trapp and Weisman 2003; Davis and Parker 2014). Despite relatively high counts of QCLSs, the central Great Plains has a comparatively

low proportion of QCLS-affiliated tornadoes, which is due to the prevalence of supercell tornadoes in this region (cf. Thompson et al. 2013, their Fig. 1a).

The most dramatic temporal signal in the tornado analysis is the comparatively higher nocturnal tendency for QCLS events versus non-QCLS events (Fig. 11c), which affirms an earlier result from Trapp et al. (2005). Nocturnal tornadoes, especially significant events, can have substantial societal impact (Ashley et al. 2008), are difficult to forecast and warn (Brotzge et al. 2013; Anderson-Frey et al. 2016), and often appear to occur in environments with ingredients not typically considered favorable for significant tornadogenesis (Kis and Straka 2010). Though tornado counts with both QCLSs and non-QCLSs reach a minimum during the overnight, the proportion that are due to QCLSs rapidly increases from less than 15% during the afternoon/evening hours to

TABLE 2. The number of tornado, severe and significant wind, and severe and significant hail reports for the 22-yr period, as well as the number and proportion of those reports attributable to QLCSSs as delineated using the spatiotemporal methods outlined in section 2c. QLCSS tornado counts and proportions are provided by increasing EF-scale damage magnitude. Reports are those from SVRGIS within the analysis domain (cf. interior rectangle in Fig. 8 panels) and where radar data were available at time of report.

Hazard	Study domain	QLCSS	% QLCSS
EF0+ tornado	24 938	5154	21%
EF1+ tornado	10 108	2899	29%
EF2+ tornado	2798	716	26%
EF3+ tornado	739	147	20%
EF4 + tornado	142	22	15%
EF5 tornado	14	0	0%
Severe wind	275 462	76 839	28%
Significant wind	18 484	6360	34%
Severe hail	247 809	24 220	10%
Significant hail	12 994	852	7%

over 50% by 0600 UTC. This majority QLCSS proportion is higher than that uncovered in the 3-yr Trapp et al. (2005) study, and does not decline notably until mid- to late morning. The population of QLCSSs is climatologically higher at night (Figs. 7a,b), which explains, at least in part, why the proportion of QLCSS tornadoes has a nocturnal maximum. Anderson-Frey et al. (2016) also found a disproportionately high ratio of nocturnal tornadoes due to QLCSSs in their analysis of the Smith et al. (2012) filtered dataset; however, their 24% proportion of nocturnal (from 2 h after sunset to sunrise) tornadoes is less than proportions found throughout most of the nocturnal hours in our analysis. We did not control for the variation in sunset/sunrise in our analysis, but from 0000 to 1200 UTC (0300–1200 UTC), the proportion of tornadoes due to QLCSSs was 28% (45%).

The 22-yr analysis has a sawtooth character to the annual proportion of *significant* (F/EF2+) tornadoes due to QLCSSs (Fig. 13a); the variability across the period is expected considering the relatively small sample size for these higher-end events. Overall, 25.6% of significant tornadoes were due to QLCSSs, with a notable increase in annual significant QLCSS tornado counts and proportions during the latter period of record. The proportion of significant tornadoes due to QLCSSs is highest from November to February, with these months exhibiting greater than 30%—and, in some cases—40% of significant tornadoes due to QLCSSs (Fig. 13b).

In a 3-yr assessment of significant nocturnal tornadoes, Kis and Straka (2010) found that 88% of the events in their sample were due to QLCSSs. Conversely, in their 9-yr analysis, Smith et al. (2012) found that less than 14% of significant nocturnal tornadoes were due to QLCSSs. This discrepancy could be due to the differences in criteria

used to delineate QLCSSs—for example, Smith et al. (2012) used a filtering method to sample events, and Kis and Straka (2010) did not include contiguous reflectivity as a part of their QLCSS delineation, suggesting that noncontiguous lines of supercells may have been included in their sample. Our methodology suggests that the proportion of significant tornadoes due to QLCSSs ranges from 50% to nearly 70% for the hourly period stretching from 0600 to 1300 UTC (Fig. 13c). Again, we did not control for the variation in sunset/sunrise in our analysis, but from 0000 to 1200 UTC (0300–1200 UTC), the proportion of significant tornadoes due to QLCSSs was 32% (50%).

Nearly 33% of QLCSSs produce at least one tornado report, with around 10% generating five or more tornadoes (Fig. 10). Over 40% of winter and spring QLCSSs produce tornadoes, while summer and fall events generate a tornado at nearly half that rate. Summer QLCSSs rarely produce large numbers of tornadoes with the 99th percentile QLCSS exceeding 10 tornadoes. Illustrating the QLCSS's propensity for tornadoes during the cool and transition seasons, only one of the top-20 QLCSSs by tornado count occurs outside of a period from late October through early May, with April the dominant mode in the top-20 list (9 of 20).

c. QLCSS severe wind occurrence

Over 28% of severe wind reports were produced by QLCSSs over the study period (Table 1). The QLCSS-attributable proportion ranges from 36% of all wind reports in 1998 and 2017 to less than 22% in 2007 (Fig. 11d). There has been a notable inflation in wind reports over the period of record; the 7-yr period from 1997 to 2003 had a mean of roughly 10 500 wind reports per year, which increased almost 38%, or to about 14 600 per year, from 2011 to 2017. Correspondingly, the number of wind reports affiliated with QLCSSs increased over the period at the same rate, with the proportion of severe wind reports due to QLCSSs remaining relatively stagnant—in the high 20s—between periods. Both QLCSS and non-QLCSS *significant* [≥ 65 kt (1 kt ≈ 0.51 m s $^{-1}$)] wind reports have trended upward during the period of record (Fig. 13d), increasing from an annual mean of under 700 reports from 1997 to 2003, to nearly 980 total reports, on average, from 2011 to 2017. These reporting trends are largely due to various biases and nonmeteorological secularities, and have been consistently trending upward for decades (Schaefer and Edwards 1999; Weiss et al. 2002; Doswell et al. 2005; Trapp et al. 2006; Smith et al. 2013; Edwards et al. 2018). Proportionally, 34% of all significant wind reports are due to QLCSSs (Table 2), with that proportion slowly increasing to 40%, on average, for the latter third of the record.

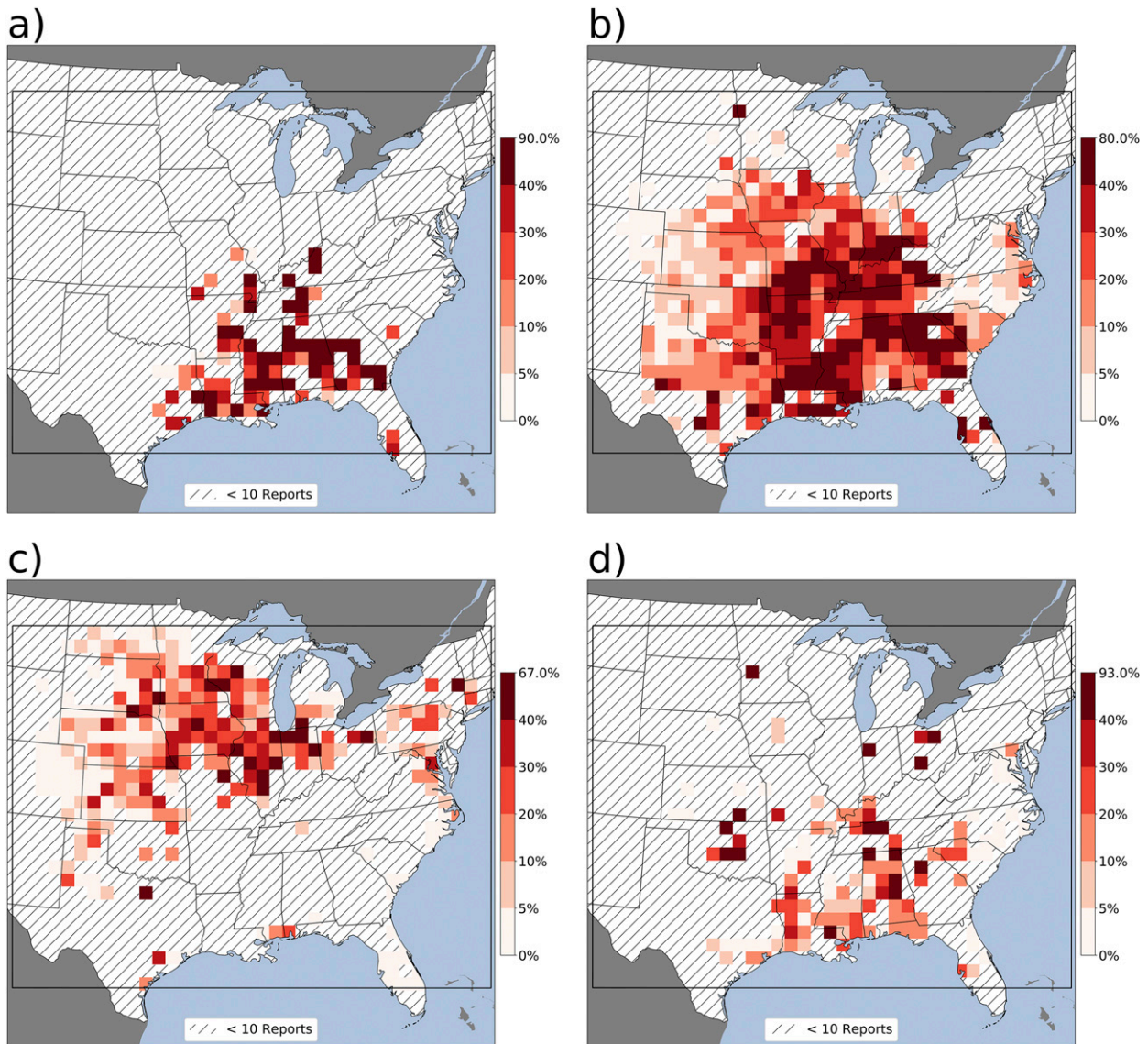


FIG. 12. As in Fig. 9, but for tornadoes.

The proportion of wind reports due to QLCS is highest in the Midwest (Fig. 8c), with over 40% of the wind reports in Arkansas, Illinois, Indiana, and Iowa due to QLCSs. A broad region including the eastern and southern Great Plains, Midwest, Ohio River Valley, and mid-South has from 30% and 50% of all wind reports due to QLCSs. Comparatively, proportional minima are found in the High Plains and along and east of the Appalachians. Wind report counts due to QLCSs maximize in May, June, and July; conversely, the proportional QLCS wind maxima occur in November (47%), January (47%), and February (58%) (Fig. 11e). Proportional QLCS wind minima occur in the latter warm-season, when unorganized convection is ubiquitous due to the

prevalence of modest instability and low-shear environments (Miller and Mote 2017). Well over 50%, to as high as 85%, of wind reports are due to QLCSs throughout most of the Southeast in the winter (Fig. 14). An even larger expanse of the central United States has over 50% of wind reports due to QLCSs during the spring, with proportional maxima constrained to the Midwest in the summer, and Midwest and Ohio River Valley in the fall. Significant severe wind reports due to QLCSs are most frequent in April–July (Fig. 13b); however, proportionally, QLCS-attributable winds prevail during the winter and spring with a majority of significant wind reports during February, March, and November due to QLCSs.

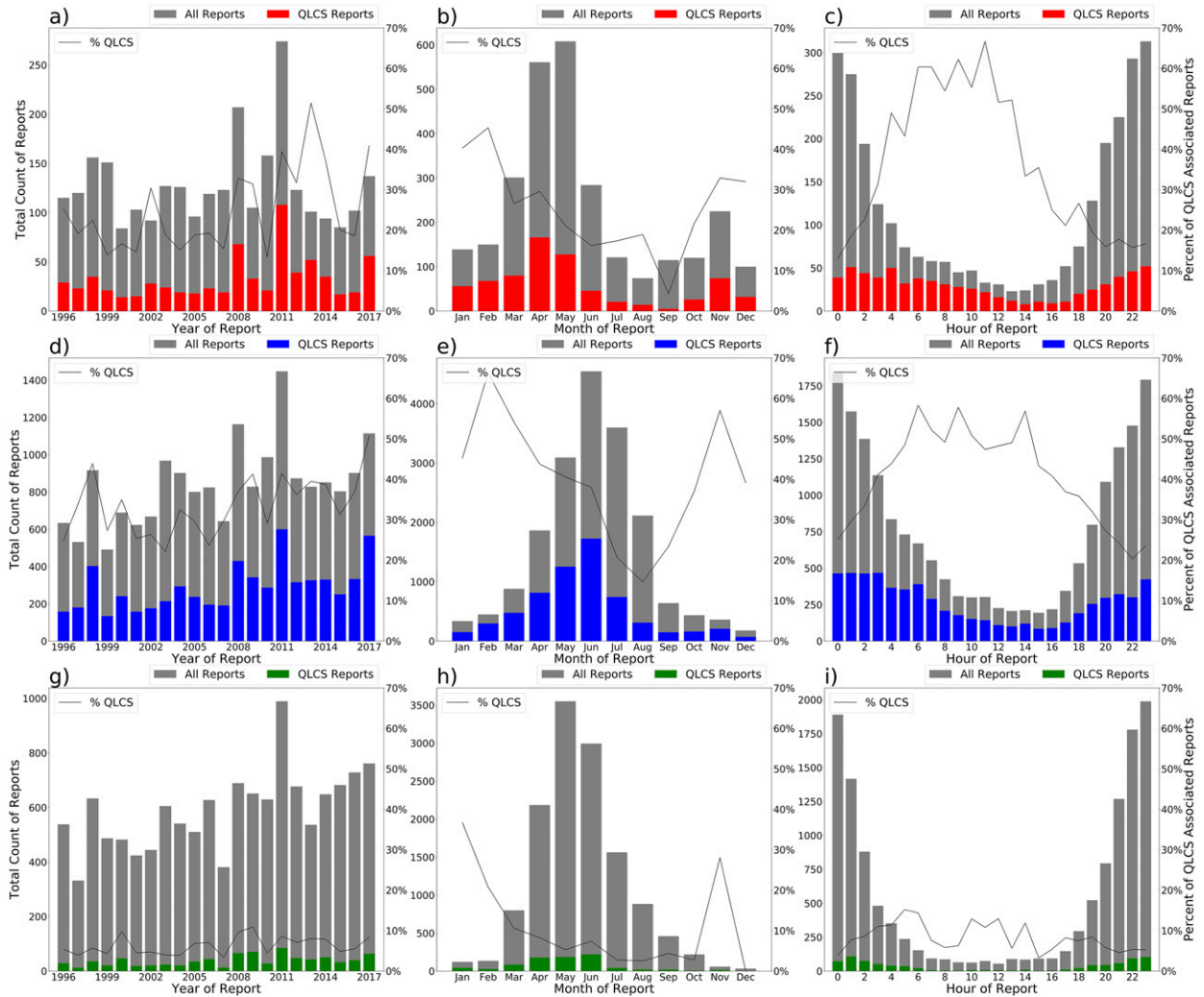


FIG. 13. As in Fig. 11, but for significant events, which include $\geq F/E/F2$ tornadoes, hail ≥ 50 mm (2 in.), and nontornadoic wind ≥ 65 kt.

Like tornadoes, the severe and significant severe wind report counts are highest (lowest) for Q LCS and non-Q LCS events during the midafternoon through evening (overnight and morning) hours (Figs. 11f and 13f). The percent of wind reports due to Q LCSs is inverse to the overall counts, increasing rapidly in proportion between 0400 and 0600 UTC and remaining above 40% through 1400 UTC. There are nearly as many, or more, Q LCS severe (significant) wind reports than non-Q LCS wind reports from 0500 to 1100 UTC (0600–1400 UTC), illustrating the importance of this organized morphology during the late-night and early morning when successful warning dissemination and implementation can be curtailed and societal impacts are high (Ashley et al. 2008; Simmons and Sutter 2009; Brotzge and Erickson 2010; Black and Ashley 2010, 2011; Mason et al. 2018).

Over 79% of Q LCS produce at least one severe and/or damaging wind report, and over 30% of events produce

at least 20 wind reports (Fig. 10). This is the dominant severe hazard mode across all seasons for a majority of Q LCSs.

d. Q LCS severe hail occurrence

Only 10% of severe hail reports are due to Q LCSs, with an attribution low of 5.6% in 2015 and a high of 14.3% in 2017 (Fig. 11g). There were over 3 times more Q LCS severe wind reports than severe hail reports over the period; this ratio was also found by Klimowski et al. (2003) in their appraisal of severe reports from linear storm complexes over the northern High Plains. The notable inflation of counts in Q LCS tornado and severe wind reports over the study record was not found with severe hail. Proportionally, the dramatic seasonal and diurnal cycles established in the Q LCS-attributable tornado and wind data are far more muted in the severe hail data. The proportion of severe hail reports due

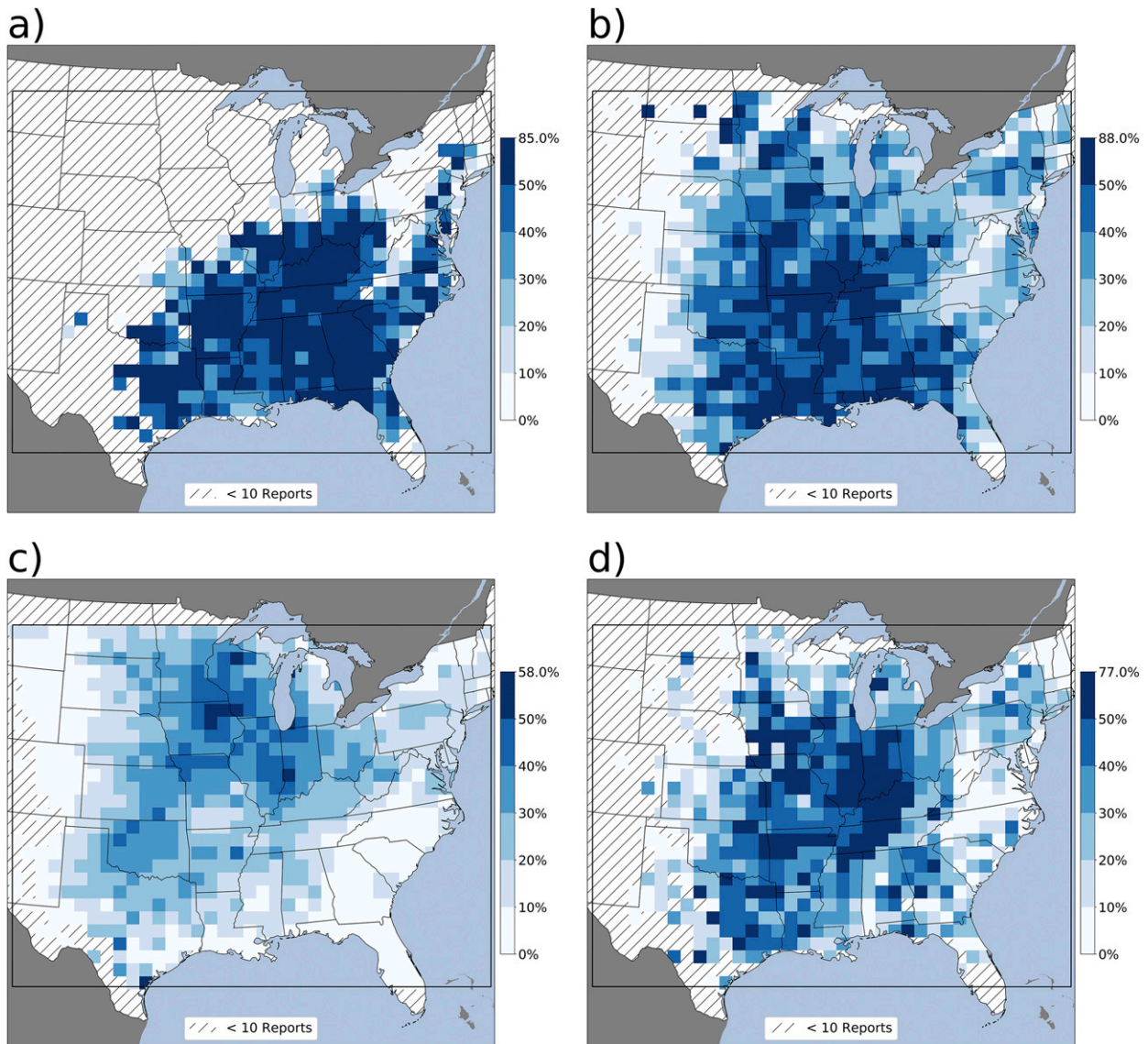


FIG. 14. As in Fig. 9, but for severe winds.

to QLCSs is maximized ($\sim 25\%$) during the winter when the overall number of severe hail reports is at a minimum (Fig. 15). While severe QLCS hail reports are most frequent in the spring and early summer, they only constitute roughly 10% of reports during this seasonal period (Fig. 11h), which suggests the supercell and other organized morphologies are the dominant severe hail producers during this season (cf. Fig. 18 in Smith et al. 2012). Spatially, the proportion of QLCS severe hail reports are generally like severe wind, but overall dampened and more varied across regional maxima due to relatively small sample sizes in bins (Figs. 8d and 15). There were only 852 *significant* (≥ 2 in.) hail reports due to QLCSs during the 22-yr period, which is only 7% of

all significant reports (Table 2). There are relatively few temporal trends, if any, in the QLCS-attributable significant hail data, which is affected by small sample size issues (Figs. 13g–i).

5. Conclusions

This research employed a QLCS-detection and tracking algorithm on more than two decades of radar imagery to generate the first, long-term, systematic climatology of QLCSs and their affiliated hazards across the United States. We used the MCS-detection algorithm developed initially in Haberlie and Ashley (2018a,b), in combination with image classification and machine

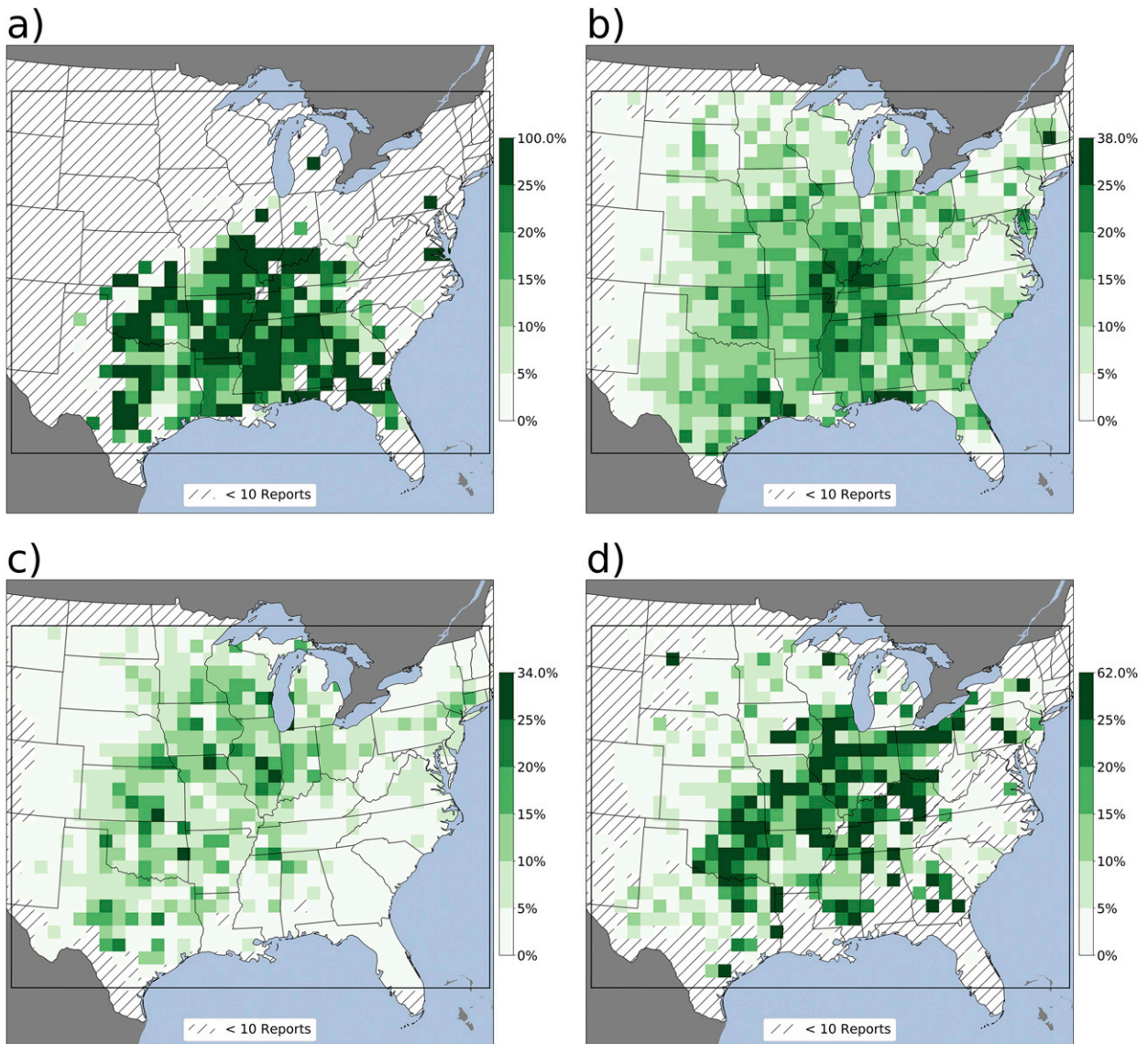


FIG. 15. As in Fig. 9, but for severe hail.

learning approaches, to advance an efficient method for detecting QLCS slices, swaths, and severe hazard reports. Expert-identified QLCSs in sample MCS-slice data informed the machine learning algorithm, which, when combined with strict, objectively applied spatiotemporal thresholds in reflectivity imagery, promoted a robust algorithm that had high accuracy in a data augmentation test. An automated method was desired because of the considerable number of MCS slices (265 953), QLCS slices (124 984), and QLCS swaths (>3000) detected using nearly 800 000 CONUS-scale radar reflectivity images at roughly 2-km, 15-min resolution. In addition, nearly 550 000 severe thunderstorm reports were considered in an attribution scheme used to assign reports to their

parent QLCS. This approach permitted an extensive assessment of the spatiotemporal climatology of QLCSs in the United States, as well as an appraisal of the amount and proportion of reported severe storm hazards due to these large, organized structures.

Results revealed that QLCSs are most frequent across the central United States, in a region stretching from the Midwest equatorward to the central Gulf Coast, and from the Interstate-35 corridor eastward to the central Ohio River Valley. Areas within this broad maximum experience, on average, 12–16 events annually, though there was notable annual variability in counts driven by late spring and early summer event populations. Overall, QLCSs were responsible for over 21% of reported

tornadoes, 28% of severe winds, and 10% severe hail across the central and eastern United States. QLCS-attributed hazard report counts and proportions were spatiotemporally diverse. QLCS tornado and severe wind reports were most frequent in the spring and early summer, and, diurnally, during the late afternoon and early evening hours. However, the proportion of tornado and severe wind reports had notable cool season and nocturnal peaks, revealing that this morphology dominates temporally when warning efficacy is diminished (Simmons and Sutter 2009; Brotzge and Erickson 2010; Mason et al. 2018). Roughly 29%–38% of MCSs are QLCSs annually, which suggests that QLCS populations and their variability have important implications for the U.S. hydroclimate, as well (Haberlie and Ashley 2019).

These results build on earlier work that has examined these storms in a subjective framework, assessing relatively short temporal periods and/or small spatial domains (e.g., Parker and Johnson 2000; Burke and Schultz 2004; Trapp et al. 2005; Gallus et al. 2008; Duda and Gallus 2010) and/or using significant severe report filtering methods (e.g., Smith et al. 2012, 2013; Anderson-Frey et al. 2016). The approach advanced here reduces the need for time-consuming expert classifications using vast amounts of data, and, instead, promotes uniform capturing of events that reduces biases that may enter assessments using subjective classification schemes. While the storm report attribution method employed herein is not faultless, we find the algorithm accuracy encouraging. Human observers have the advantage of fuzzy mental segmentation, buffer ranges, and other ad hoc decisions. The universal heuristics applied in this study represent a predictable and repeatable balance between capturing legitimate storm reports ahead of the line (e.g., outflow-induced severe wind) and overcounting some events (e.g., EF3+ tornadoes). We show that much of the results are in-line with previous work, which is a notable incremental development of the application of image classification and machine learning in meteorological and hazards research. Future work will continue to improve the detection/tracking and storm-attribution algorithms by incorporating additional data such as rotation tracks; enhancing methods that manage challenging segmentation, bridging, and buffer-related issues, especially in mixed-mode cases (e.g., merging supercell into QLCS); and incorporating additional expert judgements.

As new radar data and storm reports are accumulated, this research framework permits straightforward expansion of the climatology. Further, the method could be used in an operational setting to support efficient detection of events in simulated reflectivity output, as well as promote verification of forecasts (e.g., Pinto et al. 2015;

Ahijevych et al. 2016). Finally, we plan to use the methods and baseline climatology presented to assess and compare how these events and their hazards may evolve in the future. Using high-resolution, downscaled climate simulation output, we intend to assess how QLCS populations may change or shift in a warming climate, though the accurate simulation of MCS morphologies and their features in models remains an issue (e.g., Lawson and Gallus 2016; Grunzke and Evans 2017), especially for QLCSs (Haberlie and Ashley 2018c). Through simulation improvements, ensemble approaches, and increasing computer processing power, we can uncover the future climatology of these and similar convective events, generating information that will assist in preparation and mitigation of organized convection and its hazards in a setting featuring both significant environmental and societal changes (Tippett et al. 2015; Strader et al. 2017a,b).

Acknowledgments. We thank Russ Schumacher (CSU), Victor Gensini (NIU), David Changnon (NIU), and Bryan Smith (SPC) for their suggestions and insight that improved the research. We want to thank Arthur Person (Senior Research Assistant at The Pennsylvania State University) for providing computational resources. We also thank Matthew Bunkers, Jim Sieveking, and two anonymous reviewers whose recommendations and feedback strengthened the manuscript. This research was supported by National Science Foundation Grant ATM-1637225. This work used resources of the Center for Research Computing and Data at Northern Illinois University.

REFERENCES

- Ahijevych, D., J. O. Pinto, J. K. Williams, and M. Steiner, 2016: Probabilistic forecasts of mesoscale convective system initiation using the random forest data mining technique. *Wea. Forecasting*, **31**, 581–599, <https://doi.org/10.1175/WAF-D-15-0113.1>.
- Anderson, C. J., and R. W. Arritt, 1998: Mesoscale convective complexes and persistent elongated convective systems over the United States during 1992 and 1993. *Mon. Wea. Rev.*, **126**, 578–599, [https://doi.org/10.1175/1520-0493\(1998\)126<0578:MCCAPE>2.0.CO;2](https://doi.org/10.1175/1520-0493(1998)126<0578:MCCAPE>2.0.CO;2).
- Anderson-Frey, A. K., Y. P. Richardson, A. R. Dean, R. L. Thompson, and B. T. Smith, 2016: Investigation of near-storm environments for tornado events and warnings. *Wea. Forecasting*, **31**, 1771–1790, <https://doi.org/10.1175/WAF-D-16-0046.1>.
- Ashley, W. S., T. L. Mote, and M. L. Bentley, 2005: On the episodic nature of derecho-producing convective systems in the United States. *Int. J. Climatol.*, **25**, 1915–1932, <https://doi.org/10.1002/joc.1229>.
- , —, and —, 2007: An extensive episode of derecho-producing convective systems in the United States during May–June 1998: A multi-scale analysis and review. *Meteor. Appl.*, **14**, 227–244, <https://doi.org/10.1002/met.23>.

- , A. J. Krmenc, and R. Schwantes, 2008: Vulnerability due to nocturnal tornadoes. *Wea. Forecasting*, **23**, 795–807, <https://doi.org/10.1175/2008WAF2222132.1>.
- Atkins, N. T., C. S. Bouchard, R. W. Przybylinski, R. J. Trapp, and G. Schmock, 2005: Damaging surface wind mechanisms within the 10 June 2003 Saint Louis bow echo during BAMEX. *Mon. Wea. Rev.*, **133**, 2275–2296, <https://doi.org/10.1175/MWR2973.1>.
- Belmecheri, S., F. Babst, A. R. Hudson, J. Betancourt, and V. Trouet, 2017: Northern Hemisphere jet stream position indices as diagnostic tools for climate and ecosystem dynamics. *Earth Interact.*, **21**, <https://doi.org/10.1175/EI-D-16-0023.1>.
- Bengtsson, L., K. I. Hodges, and E. Roeckner, 2006: Storm tracks and climate change. *J. Climate*, **19**, 3518–3543, <https://doi.org/10.1175/JCLI3815.1>.
- Black, A. W., and W. S. Ashley, 2010: Nontornadoic convective wind fatalities in the United States. *Nat. Hazards*, **54**, 355–366, <https://doi.org/10.1007/s11069-009-9472-2>.
- , and —, 2011: The relationship between tornadic and nontornadoic convective wind fatalities and warnings. *Wea. Climate Soc.*, **3**, 31–47, <https://doi.org/10.1175/2010WCAS1094.1>.
- Blake, B. T., D. B. Parsons, K. R. Haghi, and S. G. Castleberry, 2017: The structure, evolution, and dynamics of a nocturnal convective system simulated using the WRF-ARW Model. *Mon. Wea. Rev.*, **145**, 3179–3201, <https://doi.org/10.1175/MWR-D-16-0360.1>.
- Bluestein, H. B., and M. H. Jain, 1985: Formation of mesoscale lines of precipitation: Severe squall lines in Oklahoma during the spring. *J. Atmos. Sci.*, **42**, 1711–1732, [https://doi.org/10.1175/1520-0469\(1985\)042<1711:FOMLOP>2.0.CO;2](https://doi.org/10.1175/1520-0469(1985)042<1711:FOMLOP>2.0.CO;2).
- Bosart, L. F., W. E. Bracken, A. Seimon, J. W. Cannon, K. D. LaPenta, and J. S. Quinlan, 1999: The evolution of warm season continental anticyclones and their contribution to derecho environments. Preprints, *17th Conf. on Weather and Forecasting*, Denver, CO, Amer. Meteor. Soc., 100–103.
- Branick, M., 1996: A comprehensive glossary of weather terms for storm spotters. 2nd ed. NOAA Tech. Memo. NWS SR-145, 49 pp.
- Brooks, H. E., and N. Dotzek, 2007: The spatial distribution of severe convective storms and an analysis of their secular changes. *Climate Extremes and Society*, H. F. Diaz and R. Murnane, Eds., Cambridge University Press, 35–53.
- Brotzge, J., and S. Erickson, 2010: Tornadoes without NWS warning. *Wea. Forecasting*, **25**, 159–172, <https://doi.org/10.1175/2009WAF2222270.1>.
- , S. E. Nelson, R. L. Thompson, and B. T. Smith, 2013: Tornado probability of detection and lead time as a function of convective mode and environmental parameters. *Wea. Forecasting*, **28**, 1261–1276, <https://doi.org/10.1175/WAF-D-12-00119.1>.
- Burke, P. C., and D. M. Schultz, 2004: A 4-yr climatology of cold-season bow echoes over the continental United States. *Wea. Forecasting*, **19**, 1061–1074, <https://doi.org/10.1175/811.1>.
- Carbone, R. E., and J. D. Tuttle, 2008: Rainfall occurrence in the U.S. warm season: The diurnal cycle. *J. Climate*, **21**, 4132–4146, <https://doi.org/10.1175/2008JCLI2275.1>.
- , J. W. Conway, N. A. Crook, and M. W. Moncrieff, 1990: The generation and propagation of a nocturnal squall line. Part I: Observations and implications for mesoscale predictability. *Mon. Wea. Rev.*, **118**, 26–49, [https://doi.org/10.1175/1520-0493\(1990\)118<0026:TGAPOA>2.0.CO;2](https://doi.org/10.1175/1520-0493(1990)118<0026:TGAPOA>2.0.CO;2).
- , J. D. Tuttle, D. A. Ahijevych, and S. B. Trier, 2002: Inferences of predictability associated with warm season precipitation episodes. *J. Atmos. Sci.*, **59**, 2033–2056, [https://doi.org/10.1175/1520-0469\(2002\)059<2033:IOPAWW>2.0.CO;2](https://doi.org/10.1175/1520-0469(2002)059<2033:IOPAWW>2.0.CO;2).
- Chrisman, J. N., 2014: The continuing evolution of dynamic scanning. *NEXRAD Now*, No. 23, NOAA/NWS/Radar Operations Center, Norman, OK, 8–13, <http://www.roc.noaa.gov/WSR88D/PublicDocs/NNOW/NNOW23a.pdf>.
- Cohen, A. E., M. C. Coniglio, S. F. Corfidi, and S. J. Corfidi, 2007: Discrimination of mesoscale convective system environments using sounding observations. *Wea. Forecasting*, **22**, 1045–1062, <https://doi.org/10.1175/WAF1040.1>.
- Coniglio, M. C., and D. J. Stensrud, 2004: Interpreting the climatology of derechos. *Wea. Forecasting*, **19**, 595–605, [https://doi.org/10.1175/1520-0434\(2004\)019<0595:ITCOD>2.0.CO;2](https://doi.org/10.1175/1520-0434(2004)019<0595:ITCOD>2.0.CO;2).
- , —, and M. B. Richman, 2004: An observational study of derecho-producing convective systems. *Wea. Forecasting*, **19**, 320–337, [https://doi.org/10.1175/1520-0434\(2004\)019<0320:AOSODC>2.0.CO;2](https://doi.org/10.1175/1520-0434(2004)019<0320:AOSODC>2.0.CO;2).
- , —, and L. J. Wicker, 2006: Effects of upper-level shear on the structure and maintenance of strong quasi-linear mesoscale convective systems. *J. Atmos. Sci.*, **63**, 1231–1252, <https://doi.org/10.1175/JAS3681.1>.
- , J. Y. Hwang, and D. J. Stensrud, 2010: Environmental factors in the upscale growth and longevity of MCSs derived from Rapid Update Cycle analyses. *Mon. Wea. Rev.*, **138**, 3514–3539, <https://doi.org/10.1175/2010MWR3233.1>.
- Corfidi, S. F., M. C. Coniglio, A. E. Cohen, and C. M. Mead, 2016a: A proposed revision to the definition of “derecho.” *Bull. Amer. Meteor. Soc.*, **97**, 935–949, <https://doi.org/10.1175/BAMS-D-14-00254.1>.
- , R. H. Johns, and M. A. Darrow, 2016b: The Great Basin Derecho of 31 May 1994. *Wea. Forecasting*, **31**, 917–935, <https://doi.org/10.1175/WAF-D-15-0178.1>.
- Crook, N. A., R. Carbone, M. W. Moncrieff, and J. W. Conway, 1990: The generation and propagation of a nocturnal squall line. Part II: Numerical simulation. *Mon. Wea. Rev.*, **118**, 50–65, [https://doi.org/10.1175/1520-0493\(1990\)118<0050:TGAPOA>2.0.CO;2](https://doi.org/10.1175/1520-0493(1990)118<0050:TGAPOA>2.0.CO;2).
- Davis, C., and Coauthors, 2004: The Bow Echo and MCV experiment: Observations and opportunities. *Bull. Amer. Meteor. Soc.*, **85**, 1075–1094, <https://doi.org/10.1175/BAMS-85-8-1075>.
- Davis, J. M., and M. D. Parker, 2014: Radar climatology of tornadic and nontornadic vortices in high-shear, low-CAPE environments in the Mid-Atlantic and Southeastern United States. *Wea. Forecasting*, **29**, 828–853, <https://doi.org/10.1175/WAF-D-13-00127.1>.
- Dial, G. L., J. P. Racy, and R. L. Thompson, 2010: Short-term convective mode evolution along synoptic boundaries. *Wea. Forecasting*, **25**, 1430–1446, <https://doi.org/10.1175/2010WAF2222315.1>.
- Dieleman, S., K. W. Willett, and J. Dambre, 2015: Rotation-invariant convolutional neural networks for galaxy morphology prediction. *Mon. Not. Roy. Astron. Soc.*, **450**, 1441–1459, <https://doi.org/10.1093/mnras/stv632>.
- Doswell, C. A., III, 2001: Severe convective storms—An overview. *Severe Convective Storms, Meteor. Monogr.*, No. 50, Amer. Meteor. Soc., 1–26.
- , and D. W. Burgess, 1988: On some issues of United States tornado climatology. *Mon. Wea. Rev.*, **116**, 495–501, [https://doi.org/10.1175/1520-0493\(1988\)116<0495:OSIOUS>2.0.CO;2](https://doi.org/10.1175/1520-0493(1988)116<0495:OSIOUS>2.0.CO;2).
- , and L. F. Bosart, 2001: Extratropical synoptic-scale processes and severe convection. *Severe Convective Storms, Meteor. Monogr.*, No. 50, Amer. Meteor. Soc., 27–69.
- , H. E. Brooks, and M. P. Kay, 2005: Climatological estimates of daily local nontornadic severe thunderstorm probability for the United States. *Wea. Forecasting*, **20**, 577–595, <https://doi.org/10.1175/WAF866.1>.

- Duda, J. D., and W. A. Gallus, 2010: Spring and summer Midwestern severe weather reports in supercells compared to other morphologies. *Wea. Forecasting*, **25**, 190–206, <https://doi.org/10.1175/2009WAF2222338.1>.
- Edwards, R., J. G. LaDue, J. T. Ferree, K. Scharfenberg, C. Maier, and W. L. Coulbourne, 2013: Tornado intensity estimation: Past, present, and future. *Bull. Amer. Meteor. Soc.*, **94**, 641–653, <https://doi.org/10.1175/BAMS-D-11-00006.1>.
- , J. T. Allen, and G. W. Carbin, 2018: Reliability and climatological impacts of convective wind estimations. *J. Appl. Meteor. Climatol.*, **57**, 1825–1845, <https://doi.org/10.1175/JAMC-D-17-0306.1>.
- Eichler, T., and W. Higgins, 2006: Climatology and ENSO-related variability of North American extratropical cyclone activity. *J. Climate*, **19**, 2076–2093, <https://doi.org/10.1175/JCLI3725.1>.
- Fabry, F., V. Meunier, B. P. Treserras, A. Cournoyer, and B. Nelson, 2017: On the climatological use of radar data mosaics: Possibilities and challenges. *Bull. Amer. Meteor. Soc.*, **98**, 2135–2148, <https://doi.org/10.1175/BAMS-D-15-00256.1>.
- Flournoy, M. D., and M. C. Coniglio, 2019: Origins of vorticity in a simulated tornadic mesovortex observed during PECAN on 6 July 2015. *Mon. Wea. Rev.*, **147**, 107–134, <https://doi.org/10.1175/MWR-D-18-0221.1>.
- French, A. J., and M. D. Parker, 2010: The response of simulated nocturnal convective systems to a developing low-level jet. *J. Atmos. Sci.*, **67**, 3384–3408, <https://doi.org/10.1175/2010JAS3329.1>.
- , and —, 2012: Observations of mergers between squall lines and isolated supercell thunderstorms. *Wea. Forecasting*, **27**, 255–278, <https://doi.org/10.1175/WAF-D-11-00058.1>.
- Fujita, T. T., 1978: Manual of downburst identification for project Nimrod. Satellite and Mesometeorology Research Paper 156, Dept. of Geophysical Sciences, University of Chicago, 104 pp. [NTIS PB-286048.]
- Galarneau, T. J., Jr., and L. F. Bosart, 2006: Ridge rollers: Mesoscale disturbances on the periphery of cutoff anticyclones. *Severe Local Storms Special Symp.*, Atlanta, GA, Amer. Meteor. Soc., P1.11, <http://ams.confex.com/ams/pdfpapers/103464.pdf>.
- , —, and A. R. Aiyyer, 2008: Closed anticyclones of the subtropics and midlatitudes: A 54-yr climatology (1950–2003) and three case studies. *Synoptic-Dynamic Meteorology and Weather Analysis and Forecasting: A Tribute to Fred Sanders*, Meteor. Monogr., No. 55, 349–392, <https://doi.org/10.1175/0065-9401-33.55.349>.
- Gallus, W. A., N. A. Snook, and E. V. Johnson, 2008: Spring and summer severe weather reports over the Midwest as a function of convective mode: A preliminary study. *Wea. Forecasting*, **23**, 101–113, <https://doi.org/10.1175/2007WAF2006120.1>.
- Geerts, B., 1998: Mesoscale convective systems in the Southeast United States during 1994–95: A survey. *Wea. Forecasting*, **13**, 860–869, [https://doi.org/10.1175/1520-0434\(1998\)013<0860:MCSITS>2.0.CO;2](https://doi.org/10.1175/1520-0434(1998)013<0860:MCSITS>2.0.CO;2).
- , and Coauthors, 2017: The 2015 Plains Elevated Convection At Night Field Project. *Bull. Amer. Meteor. Soc.*, **98**, 767–786, <https://doi.org/10.1175/BAMS-D-15-00257.1>.
- Gensini, V. A., and W. S. Ashley, 2011: Climatology of potentially severe convective environments from the North American Regional Reanalysis. *Electron. J. Severe Storms Meteor.*, **6** (8), <http://www.ejssm.org/ojs/index.php/ejssm/article/viewArticle/85>.
- Grams, J. S., R. L. Thompson, D. V. Snively, J. A. Prentice, G. M. Hodges, and L. J. Reames, 2012: A climatology and comparison of parameters for significant tornado events in the United States. *Wea. Forecasting*, **27**, 106–123, <https://doi.org/10.1175/WAF-D-11-00008.1>.
- Grunzke, C. T., and C. Evans, 2017: Predictability and dynamics of warm-core mesoscale vortex formation with the 8 May 2009 “Super Derecho” event. *Mon. Wea. Rev.*, **145**, 811–832, <https://doi.org/10.1175/MWR-D-16-0217.1>.
- Guastini, C. T., and L. F. Bosart, 2016: Analysis of a progressive derecho climatology and associated formation environments. *Mon. Wea. Rev.*, **144**, 1363–1382, <https://doi.org/10.1175/MWR-D-15-0256.1>.
- Haberlie, A. M., and W. S. Ashley, 2018a: Identifying mesoscale convective systems in radar mosaics. Part I: Segmentation and classification. *J. Appl. Meteor. Climatol.*, **57**, 1575–1598, <https://doi.org/10.1175/JAMC-D-17-0293.1>.
- , and —, 2018b: Identifying mesoscale convective systems in radar mosaics. Part II: Tracking and application. *J. Appl. Meteor. Climatol.*, **57**, 1599–1621, <https://doi.org/10.1175/JAMC-D-17-0294.1>.
- , and —, 2018c: Climatological representation of mesoscale convective systems in a dynamically downscaled climate simulation. *Int. J. Climatol.*, **39**, 1144–1153, <https://doi.org/10.1002/joc.5880>.
- , and —, 2019: A radar-based climatology of mesoscale convective systems in the United States. *J. Climate*, **32**, 1591–1606, <https://doi.org/10.1175/JCLI-D-18-0559.1>.
- Hane, C. E., J. A. Haynes, D. L. Andra, and F. H. Carr, 2008: The evolution of morning convective systems over the U.S. Great Plains during the warm season. Part II: A climatology and the influence of environmental factors. *Mon. Wea. Rev.*, **136**, 929–944, <https://doi.org/10.1175/2007MWR2016.1>.
- Heymsfield, G. M., and S. Schotz, 1985: Structure and evolution of a severe squall line over Oklahoma. *Mon. Wea. Rev.*, **113**, 1563–1589, [https://doi.org/10.1175/1520-0493\(1985\)113<1563:SAEOAS>2.0.CO;2](https://doi.org/10.1175/1520-0493(1985)113<1563:SAEOAS>2.0.CO;2).
- Higgins, R. W., Y. Yao, E. S. Yarosh, J. E. Janowiak, and K. C. Mo, 1997: Influence of the Great Plains low-level jet on summertime precipitation and moisture transport over the central United States. *J. Climate*, **10**, 481–507, [https://doi.org/10.1175/1520-0442\(1997\)010<0481:IOTGPL>2.0.CO;2](https://doi.org/10.1175/1520-0442(1997)010<0481:IOTGPL>2.0.CO;2).
- Houze, R. A., 2004: Mesoscale convective systems. *Rev. Geophys.*, **42**, RG4003, <https://doi.org/10.1029/2004RG000150>.
- , 2018: 100 Years of research on mesoscale convective systems. *A Century of Progress in Atmospheric and Related Sciences: Celebrating the American Meteorological Society Centennial*, Meteor. Monogr., No. 59, Amer. Meteor. Soc., 17.1–17.54, <https://doi.org/10.1175/AMSMONOGRAPHS-D-18-0001.1>.
- , B. F. Smull, and P. Dodge, 1990: Mesoscale organization of springtime rainstorms in Oklahoma. *Mon. Wea. Rev.*, **118**, 613–654, [https://doi.org/10.1175/1520-0493\(1990\)118<0613:MOOSRI>2.0.CO;2](https://doi.org/10.1175/1520-0493(1990)118<0613:MOOSRI>2.0.CO;2).
- Jirak, I. L., W. R. Cotton, and R. L. McAnelly, 2003: Satellite and radar survey of mesoscale convective system development. *Mon. Wea. Rev.*, **131**, 2428–2449, [https://doi.org/10.1175/1520-0493\(2003\)131<2428:SARSOM>2.0.CO;2](https://doi.org/10.1175/1520-0493(2003)131<2428:SARSOM>2.0.CO;2).
- Johns, R. H., 1982: A synoptic climatology of northwest flow severe weather outbreaks. Part I: Nature and significance. *Mon. Wea. Rev.*, **110**, 1653–1663, [https://doi.org/10.1175/1520-0493\(1982\)110<1653:ASCONF>2.0.CO;2](https://doi.org/10.1175/1520-0493(1982)110<1653:ASCONF>2.0.CO;2).
- , 1984: A synoptic climatology of northwest-flow severe weather outbreaks. Part II: Meteorological parameters and synoptic patterns. *Mon. Wea. Rev.*, **112**, 449–464, [https://doi.org/10.1175/1520-0493\(1984\)112<0449:ASCONF>2.0.CO;2](https://doi.org/10.1175/1520-0493(1984)112<0449:ASCONF>2.0.CO;2).
- , and C. A. Doswell III, 1992: Severe local storms forecasting. *Wea. Forecasting*, **7**, 588–612, [https://doi.org/10.1175/1520-0434\(1992\)007<0588:SLSF>2.0.CO;2](https://doi.org/10.1175/1520-0434(1992)007<0588:SLSF>2.0.CO;2).

- Kelly, D. L., J. T. Schaefer, and C. A. Doswell III, 1985: Climatology of nontornadic severe thunderstorm events in the United States. *Mon. Wea. Rev.*, **113**, 1997–2014, [https://doi.org/10.1175/1520-0493\(1985\)113<1997:CONSTE>2.0.CO;2](https://doi.org/10.1175/1520-0493(1985)113<1997:CONSTE>2.0.CO;2).
- Kis, A. K., and J. M. Straka, 2010: Nocturnal tornado climatology. *Wea. Forecasting*, **25**, 545–561, <https://doi.org/10.1175/2009WAF2222294.1>.
- Klimowski, B. A., M. J. Bunkers, M. R. Hjelmfelt, and J. N. Covert, 2003: Severe convective windstorms over the Northern High Plains of the United States. *Wea. Forecasting*, **18**, 502–519, [https://doi.org/10.1175/1520-0434\(2003\)18<502:SCWOTN>2.0.CO;2](https://doi.org/10.1175/1520-0434(2003)18<502:SCWOTN>2.0.CO;2).
- Krizhevsky, A., I. Sutskever, and G. E. Hinton, 2012: ImageNet classification with deep convolutional neural networks. *Advances in Neural Information Processing Systems*, Lake Tahoe, NV, Neural Information Processing Systems Conference and Workshop, 1097–1105, <http://papers.nips.cc/paper/4824-imagenet-classification-with-deep-convolutional-neural-networks.pdf>.
- Kumjian, M. R., 2013: Principles and applications of dual-polarization weather radar. Part I: Description of the polarimetric radar variables. *J. Oper. Meteor.*, **1**, 226–242, <https://doi.org/10.15191/nwajom.2013.0119>.
- , J. Evans, and J. Guyer, 2006: The relationship of the Great Plains low level jet to nocturnal MCS development. *23rd Conf. on Severe Local Storms*, St. Louis, MO, Amer. Meteor. Soc., P1.11, <https://www.spc.noaa.gov/publications/evans/kumjian.pdf>.
- Ladue, J. G., 2002: The structure of a tornadic bow echo in Idaho. *21st Conf. on Severe Local Storms*, San Antonio, TX, Amer. Meteor. Soc., P13.2, https://ams.confex.com/ams/SLS_WAF_NWP/webprogram/Paper47665.html.
- , and D. S. LaDue, 2008: Modernizing how we classify thunderstorms? An operationally useful thunderstorm classification scheme. *24th Conf. on Severe Local Storms*, Savannah, GA, Amer. Meteor. Soc., P14.6, <https://ams.confex.com/ams/24SLS/webprogram/Paper142171.html>.
- Lakshmanan, V., and T. Smith, 2010: An objective method of evaluating and devising storm-tracking algorithms. *Wea. Forecasting*, **25**, 701–709, <https://doi.org/10.1175/2009WAF2222330.1>.
- Lawson, J., and W. A. Gallus, 2016: On contrasting ensemble simulations of two Great Plains bow echoes. *Wea. Forecasting*, **31**, 787–810, <https://doi.org/10.1175/WAF-D-15-0060.1>.
- Lukens, K. E., E. H. Berbery, and K. I. Hodges, 2018: The imprint of strong-storm tracks on winter weather in North America. *J. Climate*, **31**, 2057–2074, <https://doi.org/10.1175/JCLI-D-17-0420.1>.
- Markowski, P., and Y. Richardson, 2010: *Mesoscale Meteorology in Midlatitudes*. Wiley-Blackwell, 407 pp.
- Mason, L. R., K. N. Ellis, B. Winchester, and S. Schexnayder, 2018: Tornado warnings at night: Who gets the message? *Wea. Climate Soc.*, **10**, 561–568, <https://doi.org/10.1175/WCAS-D-17-0114.1>.
- Matyas, C. J., 2010: Use of ground-based radar for climate-scale studies of weather and rainfall. *Geogr. Compass*, **4**, 1218–1237, <https://doi.org/10.1111/j.1749-8198.2010.00370.x>.
- McNulty, R. P., 1995: Severe and convective weather: A Central Region forecasting challenge. *Wea. Forecasting*, **10**, 187–202, [https://doi.org/10.1175/1520-0434\(1995\)010<0187:SACWAC>2.0.CO;2](https://doi.org/10.1175/1520-0434(1995)010<0187:SACWAC>2.0.CO;2).
- Miller, P. W., and T. L. Mote, 2017: A climatology of weakly forced and pulse thunderstorms in the Southeast United States. *J. Appl. Meteor. Climatol.*, **56**, 3017–3033, <https://doi.org/10.1175/JAMC-D-17-0005.1>.
- Myoung, B., and J. W. Nielsen-Gammon, 2010a: Sensitivity of monthly convective precipitation to environmental conditions. *J. Climate*, **23**, 166–188, <https://doi.org/10.1175/2009JCLI2792.1>.
- , and —, 2010b: The convective instability pathway to warm season drought in Texas. Part I: The role of convective inhibition and its modulation by soil moisture. *J. Climate*, **23**, 4461–4473, <https://doi.org/10.1175/2010JCLI2946.1>.
- , and —, 2010c: The convective instability pathway to warm season drought in Texas. Part II: Free-tropospheric modulation of convective inhibition. *J. Climate*, **23**, 4474–4488, <https://doi.org/10.1175/2010JCLI2947.1>.
- Newton, C. W., 1950: Structure and mechanisms of the prefrontal squall line. *J. Meteor.*, **7**, 210–222, [https://doi.org/10.1175/1520-0469\(1950\)007<0210:SAMOTP>2.0.CO;2](https://doi.org/10.1175/1520-0469(1950)007<0210:SAMOTP>2.0.CO;2).
- Nolen, R. H., 1959: A radar pattern associated with tornadoes. *Bull. Amer. Meteor. Soc.*, **40**, 277–279, <https://doi.org/10.1175/1520-0477-40.6.277>.
- Parker, M. D., and D. A. Ahijevych, 2007: Convective episodes in the east-central United States. *Mon. Wea. Rev.*, **135**, 3707–3727, <https://doi.org/10.1175/2007MWR2098.1>.
- , and R. H. Johnson, 2000: Organizational modes of mid-latitude mesoscale convective systems. *Mon. Wea. Rev.*, **128**, 3413–3436, [https://doi.org/10.1175/1520-0493\(2001\)129<3413:OMOMMC>2.0.CO;2](https://doi.org/10.1175/1520-0493(2001)129<3413:OMOMMC>2.0.CO;2).
- , and J. C. Knievel, 2005: Do meteorologists suppress thunderstorms?: Radar-derived statistics and the behavior of moist convection. *Bull. Amer. Meteor. Soc.*, **86**, 341–358, <https://doi.org/10.1175/BAMS-86-3-341>.
- Pinto, J. O., J. A. Grim, and M. Steiner, 2015: Assessment of the High-Resolution Rapid Refresh Model's ability to predict mesoscale convective systems using object-based evaluation. *Wea. Forecasting*, **30**, 892–913, <https://doi.org/10.1175/WAF-D-14-00118.1>.
- Pokharel, B., S.-Y. Wang, J. D. Meyer, R. R. Gillies, and Y.-H. Lin, 2019: Climate of the weakly-forced yet high-impact convective storms throughout the Ohio River Valley and Mid-Atlantic United States. *Climate Dyn.*, **52**, 5709–5721, <https://doi.org/10.1007/s00382-018-4472-0>.
- Przybylinski, R. W., 1995: The bow echo: Observations, numerical simulations, and severe weather detection methods. *Wea. Forecasting*, **10**, 203–218, [https://doi.org/10.1175/1520-0434\(1995\)010<0203:TBEONS>2.0.CO;2](https://doi.org/10.1175/1520-0434(1995)010<0203:TBEONS>2.0.CO;2).
- Ribeiro, B. Z., and L. F. Bosart, 2018: Elevated mixed layers and associated severe thunderstorm environments in South and North America. *Mon. Wea. Rev.*, **146**, 3–28, <https://doi.org/10.1175/MWR-D-17-0121.1>.
- Rudeva, I., and S. K. Gulev, 2007: Climatology of cyclone size characteristics and their changes during the cyclone life cycle. *Mon. Wea. Rev.*, **135**, 2568–2587, <https://doi.org/10.1175/MWR3420.1>.
- Schaefer, J. T., and R. Edwards, 1999: The SPC tornado/severe thunderstorm database. Preprints, *11th Conf. on Applied Climatology*, Dallas, TX, Amer. Meteor. Soc., 215–220.
- Schaumann, J. S., and R. W. Przybylinski, 2012: Operational application of 0–3 km bulk shear vectors in assessing quasi-linear convective system mesovortex and tornado potential. *26th Conf. on Severe Local Storms*, Nashville, TN, Amer. Meteor. Soc., 142, <https://ams.confex.com/ams/26SLS/webprogram/Paper212008.html>.
- Schenkman, A. D., and M. Xue, 2016: Bow-echo mesovortices: A review. *Atmos. Res.*, **170**, 1–13, <https://doi.org/10.1016/j.atmosres.2015.11.003>.
- , —, and A. Shapiro, 2012: Tornadogenesis in a simulated mesovortex within a mesoscale convective system. *J. Atmos. Sci.*, **69**, 3372–3390, <https://doi.org/10.1175/JAS-D-12-038.1>.
- Schoen, J., and W. S. Ashley, 2011: A climatology of fatal convective wind events by storm type. *Wea. Forecasting*, **26**, 109–121, <https://doi.org/10.1175/2010WAF2222428.1>.

- Schumacher, R. S., and R. H. Johnson, 2006: Characteristics of U.S. extreme rain events during 1999–2003. *Wea. Forecasting*, **21**, 69–85, <https://doi.org/10.1175/WAF900.1>.
- Shafer, C. M., and C. A. Doswell III, 2011: Using kernel density estimation to identify, rank, and classify severe weather outbreak events. *Electron. J. Severe Storms Meteor*, **6** (2), <http://www.ejssm.org/ojs/index.php/ejssm/article/viewArticle/74>.
- Shapiro, A., E. Fedorovich, and S. Rahimi, 2016: A unified theory for the Great Plains nocturnal low-level jet. *J. Atmos. Sci.*, **73**, 3037–3057, <https://doi.org/10.1175/JAS-D-15-0307.1>.
- Sherburn, K. D., and M. D. Parker, 2014: Climatology and ingredients of significant severe convection in high-shear, low-CAPE environments. *Wea. Forecasting*, **29**, 854–877, <https://doi.org/10.1175/WAF-D-13-00041.1>.
- , —, J. R. King, and G. M. Lackmann, 2016: Composite environments of severe and nonsevere high-shear, low-CAPE convective events. *Wea. Forecasting*, **31**, 1899–1927, <https://doi.org/10.1175/WAF-D-16-0086.1>.
- Simmons, K. M., and D. Sutter, 2009: False alarms, tornado warnings, and tornado casualties. *Wea. Climate Soc.*, **1**, 38–53, <https://doi.org/10.1175/2009WCAS1005.1>.
- Skow, K. D., and C. Cogil, 2017: A high-resolution aerial survey and radar analysis of quasi-linear convective system surface vortex damage paths from 31 August 2014. *Wea. Forecasting*, **32**, 441–467, <https://doi.org/10.1175/WAF-D-16-0136.1>.
- Smith, B. T., R. L. Thompson, J. S. Grams, C. Broyles, and H. E. Brooks, 2012: Convective modes for significant severe thunderstorms in the contiguous United States. Part I: Storm classification and climatology. *Wea. Forecasting*, **27**, 1114–1135, <https://doi.org/10.1175/WAF-D-11-00115.1>.
- , T. E. Castellanos, A. C. Winters, C. M. Mead, A. R. Dean, and R. L. Thompson, 2013: Measured severe convective wind climatology and associated convective modes of thunderstorms in the contiguous United States, 2003–09. *Wea. Forecasting*, **28**, 229–236, <https://doi.org/10.1175/WAF-D-12-00096.1>.
- Smith, J. A., D. J. Seo, M. L. Baeck, and M. D. Hudlow, 1996: An intercomparison study of NEXRAD precipitation estimates. *Water Resour. Res.*, **32**, 2035–2045, <https://doi.org/10.1029/96WR00270>.
- Stensrud, D. J., and J. M. Fritsch, 1993: Mesoscale convective systems in weakly forced large-scale environments. Part I: Observations. *Mon. Wea. Rev.*, **121**, 3326–3344, [https://doi.org/10.1175/1520-0493\(1993\)121<3326:MCSIWF>2.0.CO;2](https://doi.org/10.1175/1520-0493(1993)121<3326:MCSIWF>2.0.CO;2).
- Stoelinga, M. T., J. D. Locatelli, R. D. Schwartz, and P. V. Hobbs, 2003: Is a cold pool necessary for the maintenance of a squall line produced by a cold front aloft? *Mon. Wea. Rev.*, **131**, 95–115, [https://doi.org/10.1175/1520-0493\(2003\)131<0095:IACPNF>2.0.CO;2](https://doi.org/10.1175/1520-0493(2003)131<0095:IACPNF>2.0.CO;2).
- Strader, S. M., W. S. Ashley, A. Irizarry, and S. Hall, 2015: A climatology of tornado intensity assessments. *Meteor. Appl.*, **22**, 513–524, <https://doi.org/10.1002/met.1482>.
- , —, T. J. Pingel, and A. J. Krmenec, 2017a: Projected 21st century changes in tornado exposure, risk, and disaster potential. *Climatic Change*, **141**, 301–313, <https://doi.org/10.1007/s10584-017-1905-4>.
- , —, —, and —, 2017b: Observed and projected changes in United States tornado exposure. *Wea. Climate Soc.*, **9**, 109–123, <https://doi.org/10.1175/WCAS-D-16-0041.1>.
- Thompson, R. L., B. T. Smith, J. S. Grams, A. R. Dean, and C. Broyles, 2012: Convective modes for significant severe thunderstorms in the contiguous United States. Part II: Supercell and QLCS tornado environments. *Wea. Forecasting*, **27**, 1136–1154, <https://doi.org/10.1175/WAF-D-11-00116.1>.
- , —, A. R. Dean, and P. T. Marsh, 2013: Spatial distributions of tornadic near-storm environments by convective mode. *Electron. J. Severe Storms Meteor*, **8** (5), <http://www.ejssm.org/ojs/index.php/ejssm/article/viewArticle/125>.
- , and Coauthors, 2017: Tornado damage rating probabilities derived from WSR-88D data. *Wea. Forecasting*, **32**, 1509–1528, <https://doi.org/10.1175/WAF-D-17-0004.1>.
- Tippett, M. K., J. T. Allen, V. A. Gensini, and H. E. Brooks, 2015: Climate and hazardous convective weather. *Curr. Climate Change Rep.*, **1**, 60–73, <https://doi.org/10.1007/s40641-015-0006-6>.
- Trapp, R. J., 2013: *Mesoscale-Convective Processes in the Atmosphere*. Cambridge University Press, 346 pp.
- , and M. L. Weisman, 2003: Low-level mesovortices within squall lines and bow echoes. Part II: Their genesis and implications. *Mon. Wea. Rev.*, **131**, 2804–2817, [https://doi.org/10.1175/1520-0493\(2003\)131<2804:LMWSLA>2.0.CO;2](https://doi.org/10.1175/1520-0493(2003)131<2804:LMWSLA>2.0.CO;2).
- , S. A. Tessendorf, E. S. Godfrey, and H. E. Brooks, 2005: Tornadoes from squall lines and bow echoes. Part I: Climatological distribution. *Wea. Forecasting*, **20**, 23–34, <https://doi.org/10.1175/WAF-835.1>.
- , D. M. Wheatley, N. T. Atkins, R. W. Przybilinski, and R. Wolf, 2006: Buyer beware: Some words of caution on the use of severe wind reports in postevent assessment and research. *Wea. Forecasting*, **21**, 408–415, <https://doi.org/10.1175/WAF925.1>.
- Trier, S. B., and C. A. Davis, 2007: Mesoscale convective vortices observed during BAMEX. Part II: Influences on secondary deep convection. *Mon. Wea. Rev.*, **135**, 2051–2075, <https://doi.org/10.1175/MWR3399.1>.
- , —, and D. A. Ahijevych, 2010: Environmental controls on the simulated diurnal cycle of warm-season precipitation in the continental United States. *J. Atmos. Sci.*, **67**, 1066–1090, <https://doi.org/10.1175/2009JAS3247.1>.
- Vasiloff, S. V., 2001: Improving tornado warnings with the Federal Aviation Administration’s Terminal Doppler Weather Radar. *Bull. Amer. Meteor. Soc.*, **82**, 861–874, [https://doi.org/10.1175/1520-0477\(2001\)082<0861:ITWWTTF>2.3.CO;2](https://doi.org/10.1175/1520-0477(2001)082<0861:ITWWTTF>2.3.CO;2).
- Wakimoto, R. M., 2001: Convectively driven high-wind events. *Severe Convective Storms, Meteor. Monogr.*, No. 50, Amer. Meteor. Soc., 255–298.
- , H. V. Murphey, C. A. Davis, and N. T. Atkins, 2006: High winds generated by bow echoes. Part II: The relationship between the mesovortices and damaging straight-line winds. *Mon. Wea. Rev.*, **134**, 2813–2829, <https://doi.org/10.1175/MWR3216.1>.
- , and Coauthors, 2016: Aerial damage survey of the 2013 El Reno tornado combined with mobile radar data. *Mon. Wea. Rev.*, **144**, 1749–1776, <https://doi.org/10.1175/MWR-D-15-0367.1>.
- Wang, S.-Y., T. C. Chen, and J. Correia, 2011: Climatology of summer midtropospheric perturbations in the U.S. northern plains. Part I: influence on northwest flow severe weather outbreaks. *Climate Dyn.*, **36**, 793–810, <https://doi.org/10.1007/s00382-009-0696-3>.
- Weisman, M. L., 1992: The genesis of severe long-lived bow echoes. *J. Atmos. Sci.*, **49**, 1826–1847, [https://doi.org/10.1175/1520-0469\(1992\)049<1826:TROCGR>2.0.CO;2](https://doi.org/10.1175/1520-0469(1992)049<1826:TROCGR>2.0.CO;2).
- , 2001: Bow Echoes: A tribute to T. T. Fujita. *Bull. Amer. Meteor. Soc.*, **82**, 97–116, [https://doi.org/10.1175/1520-0477\(2001\)082<0097:BEATTT>2.3.CO;2](https://doi.org/10.1175/1520-0477(2001)082<0097:BEATTT>2.3.CO;2).

- , and C. A. Davis, 1998: Mechanisms for the generation of mesoscale vortices within quasi-linear convective systems. *J. Atmos. Sci.*, **55**, 2603–2622, [https://doi.org/10.1175/1520-0469\(1998\)055<2603:MFTGOM>2.0.CO;2](https://doi.org/10.1175/1520-0469(1998)055<2603:MFTGOM>2.0.CO;2).
- , and R. Rotunno, 2004: “A theory for strong long-lived squall lines” revisited. *J. Atmos. Sci.*, **61**, 361–382, [https://doi.org/10.1175/1520-0469\(2004\)061<0361:ATFSLS>2.0.CO;2](https://doi.org/10.1175/1520-0469(2004)061<0361:ATFSLS>2.0.CO;2).
- Weiss, S. J., J. A. Hart, and P. R. Janish, 2002: An examination of severe thunderstorm wind report climatology: 1970–1999. Preprints, *21st Conf. on Severe Local Storms*, San Antonio, TX, Amer. Meteor. Soc., 11B.2, <https://ams.confex.com/ams/pdfpapers/47494.pdf>.
- Whittaker, L. M., and L. H. Horn, 1984: Northern Hemisphere extratropical cyclone activity for four mid-season months. *J. Climatol.*, **4**, 297–310, <https://doi.org/10.1002/joc.3370040307>.
- Wurman, J., K. Kosiba, P. Robinson, and T. Marshall, 2014: The role of multiple-vortex tornado structure in causing storm researcher fatalities. *Bull. Amer. Meteor. Soc.*, **95**, 31–45, <https://doi.org/10.1175/BAMS-D-13-00221.1>.